wileyonlinelibrary.com/journal/luminescence

LUMINESCENCE
The Journal of Biological and Chemical Luminescence

Volume 27 Number 3
May–June 2012

Featured article

(wileyonlinelibrary.com) DOI 10.1002/bio.2342

High-field magneto-photoluminescence of semiconductor nanostructures

Manus Hayne and Bhavtosh Bansal

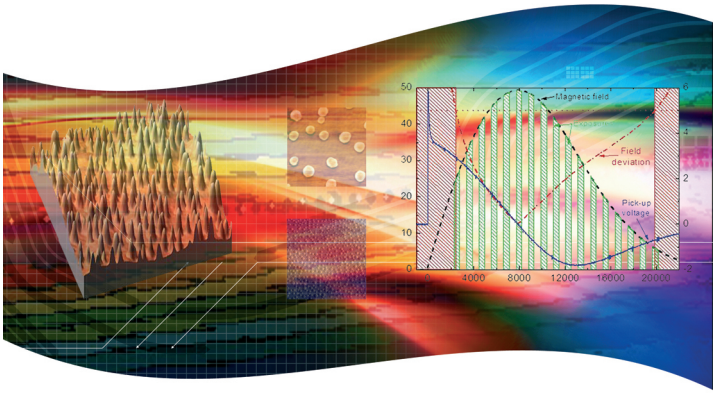

This month's featured perspective article; "High-field magneto-photoluminescence of semiconductor nanostructures" is authored by Manus Hayne and Bhavtosh Bansal. The perspective reviews the photoluminescence of semiconductor nanostructures in high magnetic fields, concentrating on the effects of the applied magnetic field on orbital motion (wave function extent), which is probed in experiments on large ensembles.

The cover of this issue of Luminescence features a graph of the shutter sequence for 0.5-ms exposures at 17 different field values for an InGaAs linear array with 0.5-ms readout time as detector.

Authors' Biography

Manus Hayne graduated with a BSc in Physics with Electronics from the University of Southampton and a PhD in Physics from the University of Exeter, both in the United Kingdom. He was a post-doctoral researcher at the University of Exeter, the Laboratoire de Microstructure et de Microélectronique (now Laboratoire de Photoniques et de Nanostructures), France, and the Katholieke Universiteit Leuven, Belgium. He is presently a Senior Lecturer in the Department of Physics, Lancaster University. His research interests are in the physics and applications of low-dimensional III-V compound semiconductor materials.

Bhavtosh Bansal studied up to his Masters at the University of Delhi and then moved to the Indian Institute of Science, Bengaluru, India for a PhD in experimental semiconductor physics. After postdocs at Tata Institute of Fundamental Research, Mumbai, India, Katholieke Universiteit Leuven, Belgium and the High Field Magnet Laboratory, Nijmegen, The Netherlands, he is currently an Assistant Professor at the Indian Institute of Science Education and Research- Kolkata, India. Along with colleagues, at the moment he is busy building up a small pulsed field laboratory and a semiconductor spectroscopy laboratory. Current research interests include excitons in nanostructures and physics in high magnetic fields.

Special feature: review

LUMINESCENCE
The Journal of Biological and Chemical Luminescence

Published online in Wiley Online Library

(wileyonlinelibrary.com) DOI 10.1002/bio.2342

High-field magneto-photoluminescence of semiconductor nanostructures

Manus Hayne[a]* and Bhavtosh Bansal[b]

ABSTRACT: We review the photoluminescence of semiconductor nanostructures in high magnetic fields, concentrating on the effects of the applied magnetic field on orbital motion (wave function extent), which is probed in experiments on large ensembles. We present an overview of the physics of excitons in high magnetic fields in 3- and 2-D before introducing the zero-dimensional case. We then discuss the physics of quantum-dot excitons in high magnetic fields with particular attention to the approximate analytical models used to interpret experimental results. This is followed by a brief description of a typical high-field magneto-photoluminescence setup. We then present four examples of magneto-photoluminescence experiments on different materials systems chosen from our own research to illustrate how high magnetic fields can be used to reveal new insights into the physics of semiconductor nanostructures. Copyright © 2012 John Wiley & Sons, Ltd.

Keywords: photoluminescence; semiconductor nanostructures; magnetic fields; magneto-photoluminescence; solid-state physics; semiconductor quantum dots; crystalline semiconductors; excitons; high-field magneto-PL

Introduction

High magnetic fields are one of the principal research tools in solid-state physics and have been widely applied in the investigation of the optical and transport properties of bulk and low dimensional semiconductors, generating Nobel prizes for the discovery of the integer (1) and fractional quantum Hall effects (2). Semiconductor nanostructures are no exception. Indeed, it can be said that the technological interest in semiconductor quantum dots (QDs) can be traced to the influential study by Arakawa and Sakaki (3). They showed that the application of a strong magnetic field to a quantum well laser produced 3D confinement that substantially improved the temperature stability of the threshold current density with an increase in the characteristic temperature T_0 from 144 °C at 0 T to 313 °C at 30 T.

In this review, we discuss the application of high magnetic fields to semiconductor nanostructures for the investigation of their optical and electronic properties. In this context, 'high' means that the applied field does more than just perturb the orbital motion of confined carriers; i.e., the magnetic length (to be defined below) is of comparable size or smaller than the zero-field wave-function extent of the confined carriers. This occurs at fields of at least several tesla, often much more. We begin with a basic introduction to excitons in crystalline semiconductors and the physics of excitons in high magnetic fields. Next, we provide a phenomenological description of the physics of QDs in high magnetic fields, introducing analytical models that have been applied to interpret experimental data. The experimental setup for the measurement of photoluminescence (PL) in pulsed fields is described in some detail since this information is not easily accessible elsewhere. Finally, we highlight the contribution of high-field magneto-PL to research on semiconductor nanostructures with examples in four different material systems: Example 1) InP QDs in GaAs, Example 2) InAs QDs in GaAs, Example 3) Si nanocrystals in SiO_2 and Example 4) GaSb QDs in GaAs. This review aims to be a semi-pedagogical introduction; an exhaustive literature survey would require a book-length monograph. The examples were taken from our own work in the past decade and are intended to illustrate the power of the technique under various circumstances.

Physics of excitons in high magnetic fields

Introduction and background

Optical excitation of a semiconductor at an energy larger than its band gap generates a polarization (polariton) wave within the material. This polarization rapidly dephases in sub-picosecond time scales to give rise to photo-generated electron–hole pairs with nearly zero centre-of-mass momentum. Various scattering processes very quickly thermalize these electron–hole pairs to the band-edge within the time scale of a few picoseconds (4). In direct-gap semiconductors such as GaAs, InAs, InP, GaN, ZnSe and $Hg_xCd_{1-x}Te$, the electron–hole pairs were likely to recombine radiatively by emitting photons near the band-gap energy. In most bulk semiconductors, with band gaps of the order of 1 eV, the electrons and holes can be treated as independent particles. When the above-mentioned process occurs in the presence of a large magnetic field, the magnetic field independently

* Correspondence to: Manus Hayne, Department of Physics, Lancaster University, Lancaster LA1 4YB, United Kingdom.
E-mail: m.hayne@lancaster.ac.uk

[a] Department of Physics, Lancaster University, Lancaster LA1 4YB, United Kingdom

[b] Indian Institute of Science Education & Research – Kolkata, Monhanpur Campus, Nadia 741252, West Bengal, India

quantizes the electron and hole states into Landau levels. The energy spectrum of free particles of charge e and effective mass m^* under a magnetic field B applied along the z-axis (5) hence becomes equation (1):

$$E = \frac{\hbar^2 k_z^2}{2m^*} + \hbar\omega_c[n + \frac{1}{2}] + g\mu_B B_z \quad (1)$$

The first term is the parabolic dispersion in the z direction for wave vector k_z, the second is the diamagnetism associated with the Landau quantization in the plane perpendicular to the magnetic field, and the third term is the paramagnetism associated with the electron spin (Zeeman effect). $\omega_c = |eB|/m^*$ is the classical cyclotron frequency, μ_B is the Bohr magneton, and $\hbar$ is the reduced Planck constant. Landau quantization is a fundamentally quantum mechanical effect; there is no diamagnetism in classical physics due to the celebrated Bohr-von Leeuwen theorem (6). Unlike the free electron case, the g-factor can be significantly different from 2 in semiconductors and even be negative, depending not only on the material but also on the size and geometry of the heterostructure. $n = 0, 1, 2, \ldots$ is the Landau-level index corresponding to 1D harmonic oscillator-like states. Note that while the application of the magnetic field restricts the electron (or hole) motion in two dimensions (i.e., in the plane perpendicular to which it is applied), the energy spectrum in the above equation yields only a single harmonic oscillator spectrum. This apparent paradox is resolved by noting that these harmonic oscillator levels are highly degenerate and that this degeneracy accounts for the second degree of freedom that is curtailed by the magnetic field. The degeneracy of Landau levels is simply given by the number of magnetic flux quanta eB/h passing through each unit area of the sample in the plane perpendicular to the magnetic field. Similarly, the Landau-level filling factor ν is given by the number of electrons per flux quantum in any given area, noting that due to electron or heavy-hole spin degeneracy, $\nu = 2$ corresponds to one full Landau level. In very high magnetic fields, the extreme quantum limit ($\nu << 1$) is reached, which implies that all conduction-band electrons and/or valence-band holes occupy only the lowest Landau level. In PL experiments on undoped samples where electrons or holes are photo-excited carriers, their areal number density is typically low so that $\nu < < 1$ is reached at quite low magnetic fields. The form and symmetry of the wave functions obtained in high fields is highly gauge dependent but the physical observables like the expectation value of the orbit centre or the cyclotron energy are obviously not (5). Classically, charged particles execute a circular motion in the plane perpendicular to the applied field but the motion along the direction of the magnetic field is unaffected, so the overall path followed is that of a helix.

In a real experimental situation where there is always some disorder (thermal and topological), the formation of Landau levels requires that on average, the electron is likely to have completed several cyclotron orbits before it is scattered. Furthermore, experimental observation of effects related to Landau quantization also requires that temperature T be low enough so that only the lowest few Landau levels have a significant occupation probability.

These conditions can be mathematically stated (7) as $\omega_c\tau_q > 1$ and $\hbar\omega_c > k_B T$, where k_B is the Boltzmann constant and τ_q is the mean collision time, also called the quantum lifetime. τ_q differs from the collision time appearing in the expression for the electron mobility (momentum relaxation time) in that the latter is a scattering angle-dependent weighted average over scattering events. Apart from the Landau quantization energy $\hbar\omega_c$, there is also a length scale associated with Landau-quantized electron orbits, the magnetic length $l_B = \sqrt{\hbar/(eB)}$ that corresponds to the size of the classical orbit of carriers in the lowest Landau level. It is important that the magnetic length depends only on fundamental constants. More details on free-particle Landau levels can be found in quantum mechanics texts or specialized monographs on the subject such as by Miura (8).

The physics of charged particles in an applied magnetic field becomes complicated when the number of particles exceeds one; that is, when the interactions between them cannot be ignored. The fractional quantum Hall effect (2) is an extreme example of a new phase of matter, where the fundamental charge carriers themselves are not electrons as we usually encounter them, but fractionally-charged quasi-particles that have an effective charge of $e/3$ (9,10). Historically, in the context of photo-excited electrons and holes, it was debated whether the interaction between electrons and holes could ever show up in optical absorption and emission spectra (11). It is now well established that, at least at low enough temperatures, they do form bound states (excitons) whose envelope functions are (in the simplest one-band effective-mass picture) mathematically equivalent to hydrogen-atom wave functions (12).

Thus, the problem of the hydrogen atom in a magnetic field provides a good starting point for studying the physics of excitons in high magnetic fields. The ground state of the hydrogen atom has two natural scales: the Rydberg $R_H = m_0 e^4/(2\varepsilon_0^2/\hbar^2)$ (binding energy) and the Bohr radius $a_B^0 = 4\pi\varepsilon_0^2/m_0 e^2$, which are equal to 13.6 eV and 0.529 Å, respectively. m_0 is the free electron mass and ε_0 is the dielectric constant of free space. For all but astrophysical-strength magnetic fields ($B > 10^5$ T or 10^9 Gauss) (13,14), these values imply that an externally applied magnetic field is always a small perturbation to the ground state of the atomic system. Under the influence of laboratory strength magnetic fields, low-lying states of atomic systems are well described within perturbation theory. To order B^2, the change in the energy (15) is given by equation (2):

$$\Delta E_n = \mu_B \vec{B} \bullet \left\langle n \middle| \vec{L} + g\vec{S} \middle| n \right\rangle + \sum_{m \neq n} \frac{\left| \left\langle n \middle| \vec{L} + g\vec{S} \middle| m \right\rangle \right|^2}{E_m - E_n} + \frac{e^2 B^2}{8\mu} \left\langle n \middle| \sum_i (x_i^2 + y_i^2) \middle| n \right\rangle \quad (2)$$

The first two terms denote paramagnetism due to the orbital ($\vec{L}$) and spin ($\vec{S}$) angular momentum (first- and second-order Zeeman effects). The last term, the diamagnetic contribution to the energy correction, is what we will focus on in this review. This is because, for zero-angular-momentum states $\vec{L} = 0$ (as ground states usually are), the orbital paramagnetic contribution is zero while the spin contribution is often ill-resolved due to the small value of the g-factor, especially in ensemble studies of QDs where spectra are inhomogeneously broadened. The characteristic B^2 energy shift due to low-field diamagnetism is observed not just for the hydrogenic ground-state but most bound states (16). In a typical direct-gap semiconductor like GaAs, the large dielectric constant ($\varepsilon = 12.5\ \varepsilon_0$ in GaAs) and the small effective mass

LUMINESCENCE
The Journal of Biological and Chemical Luminescence

($m^* = 0.067\ m_0$ in GaAs) make the effective Bohr radius and binding energy (effective Rydberg) ~ 10.2 nm and 4.8 meV, respectively. Then, magnetic fields of a few tesla are no longer a small perturbation: strong deviations from a quadratic shift are observed at higher fields and the simple perturbation theory analysis of equation (2) no longer suffices.

The problem of hydrogen atoms and excitons in magnetic fields of arbitrary strength has a large body of theoretical work devoted to various approximations. The earliest perturbative result in the opposite, high magnetic field limit, was first developed by Elliot and Loudon in the late 1950's (17) where it was shown that for large fields when the magnetic length was much smaller than the Bohr radius, the problem could be effectively treated as a 1D hydrogen atom problem, with the other two spatial dimensions becoming completely constrained by the magnetic confinement. Before this, a rather crude variational solution to the problem in the complete range of magnetic field values was provided by Yafet *et al.* (18). The wave function was assumed to have a Gaussian form with two variational parameters corresponding to the exciton radii in the directions parallel and perpendicular to the magnetic field. Thus, although the model assumed an incorrect form for the wave function at $B = 0$ (which should be an exponential corresponding to the standard hydrogenic ground state wave function), it nevertheless captured one fundamental aspect of the problem, namely that the symmetry changes from spherical to cylindrical on application of a magnetic field.

Since the late 1970s, there has been a continuous effort to improve these variational solutions by increasing the number of parameters. The currently popular basis of many Gaussian wave functions gives almost exact results. The various variational schemes adopted over the years were reviewed by Zawadzki *et al.* in the context of the similar problem of shallow donor bound states in magnetic field (19). Numerical solutions also became popular in the 1980's, and much theoretical and experimental progress was made in understanding the detailed nature of the orbits. Figure 1 shows a nearly exact numerical calculation of the ground state energy of the hydrogen atom taken from Rosner *et al.* (20) and Xi *et al.* (21). Here, $\Gamma = \frac{\hbar\omega_c}{2R_H}$ is the dimensionless ratio of the cyclotron energy and the Rydberg energy. $\Gamma \sim 1$ corresponds to the intermediate field boundary where there is a change in slope from 2 (characteristic of diamagnetic behaviour; low field) to 1 (characteristic of Landau levels; high field). For excitons in semiconductors, the effective Rydberg is about three orders of magnitude smaller than in hydrogen due to the large static dielectric constant and small effective mass of carriers. The small effective mass also makes the cyclotron energy about 1–2 orders of magnitude larger for the same magnetic field. As a result, while $\Gamma \sim 1$ corresponds to a field of 4 x 10^5 T for a hydrogen atom, for excitons, it may be only a few tesla.

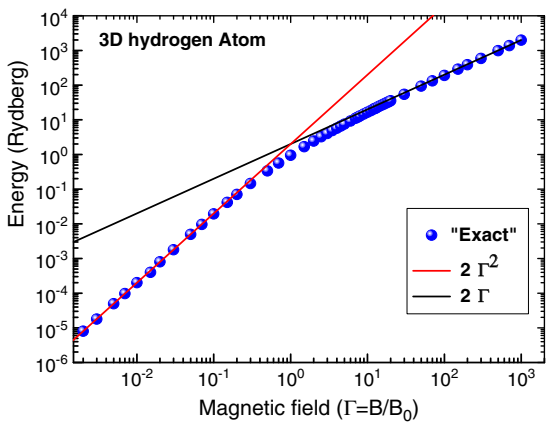

Figure 1. Circles: magnetic field dependence of the ground-state energy of the hydrogen atom as calculated numerically (after Rosner *et al.* (20) and Xi *et al.* (21)). The magnetic field is plotted in the normalized units $\Gamma = \frac{\hbar\omega_c}{2R_H}$ (see text). The low- and high-field dependence is very well described by two straight lines (on log scale) with slopes of 2 and 1, respectively. The crossover region occurs around $\Gamma = 1$

Numerically intensive though these solutions might become, physics-wise, the problem is effectively just that of solving the single-particle Schrodinger equation. Thus, the solution is in principle trivial, even if not analytic. Nevertheless, two non-trivial and interesting features do show up in the hydrogen atom problem in magnetic field. These are (i) the expected transition to quantum chaos (22) and (ii) coupling of the centre of mass and the orbital degrees of freedom leading to the motional Stark effect and decentred (giant dipole) states (23,24). These will not be discussed here since our focus is on characterization of nanostructures using high-field PL.

The two-dimensional case

Before moving on to QDs, let us present the salient features of the excitonic properties of high-field PL in quantum wells, where the electrons and holes are confined within a 2D plane. For sufficiently narrow quantum wells, ignoring the third dimension is a good approximation as long as the Landau-level energy is much smaller than inter-subband energy arising out of quantization in the third dimension. When a magnetic field is applied perpendicular to the plane of the quantum well ($B//z$, where z is the growth direction), the essential physics of the problem is unchanged from the previous 3D case except for one important qualitative difference: for a 2D system, the symmetry of the hydrogenic exciton is unaffected by the application of the magnetic field and the wave functions are expected to continuously transform from hydrogenic to harmonic-oscillator-type (Landau-level) wave functions as the magnetic field is increased. From a practical point of view, since for quantum-well excitons, the problem only involves solving the 1D radial Schrodinger equation even in high magnetic fields, the numerical calculations are easier and again, a variational calculation with a basis of many Gaussian wave functions gives very accurate results (25).

Experimentally, in 2D quantum wells, excitons are much more robust than in the bulk and can survive up to room temperature. The excitonic binding energy is expected to be four times the bulk value for a perfect 2D system, but in actual quantum wells (26), it is a bit less and dependent on the actual width of the well (27). From the early 1980s (28), there have been a large number of spectroscopic experiments (PL and PL excitation spectroscopy) on quantum wells of various materials in high magnetic fields. One scheme for analysing the magneto-PL of quantum wells, which turned out to be quite convenient for experimentalists, was due to MacDonald and Ritchie (29) who showed that the exciton energy could be fitted to a function which was a ratio of two fourth-order polynomials computed by Padé interpolation of the results of perturbation theory applied to the low- and high-magnetic field regimes. Using this method, one rescales the exciton problem into dimensionless energy and magnetic-field strength to obtain either the exciton-reduced effective mass and/or the dielectric constant. Figure 2 shows one of the authors' previously unpublished data

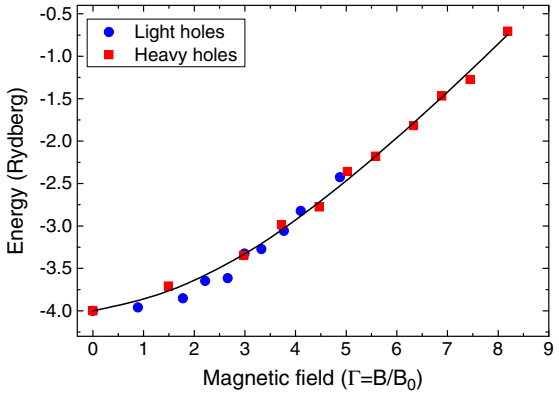

Figure 2. Solid line: magnetic field dependence of the ground state energy of the 2D hydrogen atom using the polynomial coefficients provided by MacDonald and Ritchie (31). The actual data for the heavy- (red squares) and light-hole (blue circles) excitons in a GaAs quantum well is scaled such that a best fit to this curve is obtained. In the experiment, photoconductivity from both heavy-hole and light-hole excitons peaks were measured up to 22 T

where the heavy-hole and light-hole masses for excitons in a 15-nm GaAs quantum well were deduced by the best fits of the data using the analysis of reference (29). The in-plane heavy- and light-hole exciton-reduced effective masses were found to be $0.044\,m_0$ and $0.057\,m_0$, respectively. Note that the in-plane mass of the heavy-hole is smaller than that for the light-hole due to the well-known phenomenon of mass reversal in these systems (30).

Considerable effort has also been spent on studying the physics of excitons in doped quantum wells where they can occur in various charged states such as negatively and positively charged trions. The interest was to understand optical selection rules in magnetic field and study the evolution of the binding energies of the singlet and triplet states (31–33). Optical signatures of the fractional quantum hall effect have also sobserved in magneto-PL from two-dimensional electron systems (34,35).

The problem of quantum dots in magnetic fields

In this review, we are primarily concerned with the effect of magnetic field on charges confined to self-assembled semiconductor nanostructures. A complete description of the physics of such a situation requires the application of state-of-the-art computational techniques, both to model the sample band-structure and to describe the physics in an applied magnetic field (36). Ideally, such an analysis should be used to interpret all such experimental data, but this is often not possible because there is insufficient morphological data about the samples to warrant such an approach. In such cases, approximate analytical models are justified (37), especially when inhomogeneous broadening of ensembles means that the average behaviour is observed, and besides, such approaches often allow access to the key physics. The central problem is that when constructing such models, three energies are involved: the spatial confinement energy, the Coulomb interaction energy (binding energy) of the exciton, and the cyclotron energy associated with the applied magnetic field. The binding energy of an isotropic 3D exciton E_B is given by equation (3):

$$E_B = \hbar^2/2\mu a_B^2 \tag{3}$$

where μ is the exciton reduced mass given by $\mu = \left(1/m_e^* + 1/m_h^*\right)^{-1}$ in which m_e^* and m_h^* are the effective masses of the electron and the hole respectively. a_B is the exciton Bohr radius and is equal to $a_B = a_B^0\varepsilon/(\mu/m_0)$, where $a_B^0 = 0.529$ Å is the Bohr radius of the hydrogen atom. For a heavy-hole exciton in bulk GaAs, the binding energy is ~4.8 meV, which although is an order of magnitude smaller than the typical confinement energy in self-assembled semiconductor nanostructures (40 meV is a common electron sub-band separation), is not negligible. Furthermore, confinement of excitons in nanostructures increases the binding energy by squeezing the electron and hole together in a small volume and increases the exciton mass through the effects of non-parabolicity (38,39) and strain-induced deformation of the bands in self-assembled nanostructures (40). The key idea in using high magnetic fields for characterising QDs is to make the magnetic length small enough such that it, along with the exciton Bohr radius, is also a relevant length scale in the plane perpendicular to the applied field. At 10 T $l_B = 8.1$ nm, whereas for an exciton in bulk GaAs, $a_B = 10.2$ nm. The net result is a situation where there are three comparable and competing energy scales, making the formulation of a complete analytical description of the system challenging even in the absence of an accurate description of the true confinement potential that can be included in the full numerical models referred to above.

The usual way around this is to make simplifying approximations to allow a semi-analytical approach to the problem: either the binding energy (e.g., Fock-Darwin model) or the confinement energy (e.g., excitonic model) is neglected. It turns out that both of these approximations are not as different as they might initially seem, largely because the two energies are inextricably linked; given a set of data that covers both high and low field regimes, the parameters obtained are very similar (41).

Quantum dot excitons in magnetic fields: analytical models

Fock-Darwin model

Fock-Darwin states were derived independently by Fock (42) and Darwin (43). They describe the energy levels of an electron in a 2D harmonic potential of energy $\hbar\omega_0$ in a perpendicularly applied magnetic field with radial quantum number (Landau level index) n and orbital angular momentum quantum number l ($l = 0, \pm1, \pm2, \pm3\ldots$), resulting in equation (4):

$$E_{n,l} = E_0 + (2n + |l| + 1)\hbar\sqrt{\omega_0^2 + \frac{\omega_c^2}{4}} - \frac{1}{2}l\hbar\omega_c \tag{4}$$

where E_0 is the vertical confinement energy; i.e., the confinement energy in the direction of the applied magnetic field. A typical Fock-Darwin spectrum calculated using $\hbar\omega_0 = 40$ meV and $m_e = 0.070\,m_0$ is shown in Figure 3. It can be seen that the radial quantum number n defines a series of occupancy energy levels that are analogous to the shells of an atom and are hence often labelled as s, p, d *etc.* for this reason (33,37).

The most important feature of the Fock-Darwin description when applied to PL experiments on QDs is that it is a single particle approximation; i.e., the effect of the Coulomb interaction is neglected. This not only ignores the excitonic interaction between electron and hole but also any electron–electron interactions in the case of multiple occupancy. It has been argued that the former, neglecting the excitonic nature of the problem, can be resolved by assuming that the electron and hole wave-functions have an identical form for electrons

LUMINESCENCE
The Journal of Biological and Chemical Luminescence

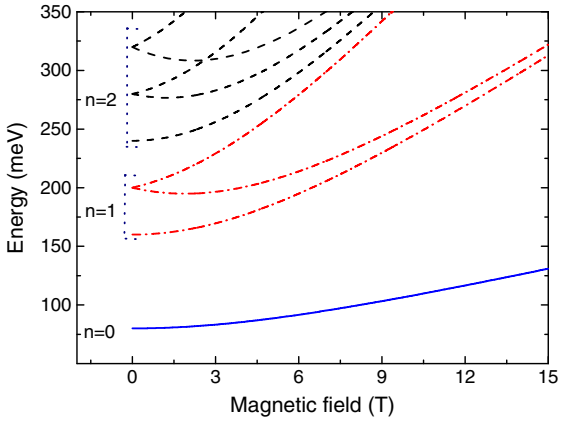

Figure 3. Calculated Fock-Darwin spectra with $\hbar\omega_0 = 40$ meV and vertical confinement energy E_0 also arbitrarily chosen to be 40 meV. The effective mass $m^* = 0.070\, m_0$. Energy levels are plotted for the principal quantum number (Landau-level index) $n = 0$, 1 and 2

and holes in equivalent levels n (44), in which case $\hbar\omega_0$ becomes the sum of the electron and hole confinement energies and the reduced exciton mass is used to find the cyclotron energy rather than the electron effective mass, and the exciton binding energy as well as the band-gap are incorporated into the term E_0, which is then equal to the PL energy in zero magnetic field (45). This definition of E_0 will be applied from hereon in. Given that the electron effective mass is typically 10 x < than that of the hole and that the valence band is much more complicated than the conduction band with the presence of heavy- and light-hole bands with a more complex dependence on strain, this is unlikely to be accurate. A second approximation is the symmetry of the confining potential, which gives degenerate excited states. In practice, this symmetry can be broken by asymmetry in the shape of the dots caused, for example, by elongation in one crystallographic direction in the plane of the sample (46) by piezoelectric effects (47) or the asymmetry in crystallographic facets at opposite sides of the dots (48). Accounting for such effects requires substantially more sophisticated models that cannot be described analytically and quite often require detailed information about the morphology of the dots to be applied correctly. Nevertheless, the Fock-Darwin approach provides a good first-order approximation description of QD states in magnetic field even when the dots are multiply-occupied (49).

Low-field and high-field limits

Just as in the 3D and 2D cases described above, for a QD in low magnetic field; i.e., when the magnetic length is much > than the size of the confined exciton wave-function (Bohr radius) in the plane perpendicular to the applied field and the cyclotron energy is small, an applied magnetic field provides a small perturbation, giving a parabolic field dependence of the energy (diamagnetic shift) if the Zeeman terms are ignored (50–52), as shown in equation (5):

$$\Delta E = \frac{e^2 a_B^2}{8\mu} B^2 \tag{5}$$

On the other hand, in the high-field limit when l_B is much smaller than the zero-field Bohr radius and where the cyclotron energy is large, the magnetic confinement of the exciton wave-function by the applied field dominates, the spatial confinement in the plane perpendicular to the applied field can be neglected and the system becomes equivalent to a 2D system with a field applied perpendicular to the plane. Hence, the energy shift is given by that of the lowest Landau level as expressed in equation (6):

$$\Delta E = \frac{1}{2}\hbar\omega_c \tag{6}$$

and is expected to be linear in B. Note that this neglects the field dependence of the binding energy. For 3D, this is weak, going as $\log B^2$ for $B \to \infty$, while for two dimensions, it goes as $\sqrt{B}$ (11,29). This description is also borne out in Figure 1 where the exact field dependence of the ground state energy of the hydrogen atom is clearly seen to asymptotically approach the slopes of 1 and 2 in the high- and the low-field regimes, respectively.

In between these two limits, there exists an intermediate field regime (Fig. 1) where the magnetic field is neither weak nor strong and is analytically most difficult to deal with. But clearly, the behaviour between the two regimes must be continuous and analytic (there is no phase transition) and some interpolation can be used to bridge the gap. In two dimensions, we mentioned that a Padé interpolation scheme between these two regimes was introduced by MacDonald and Ritchie (29).

Another interpolation was proposed by Janssens *et al.*, who numerically calculated the field dependence of the exciton energy in a quantum disk (53). They found that their numerical results were in good agreement with the empirical function (54), as shown in equation (7):

$$\Delta E = \frac{\beta B^2}{1 + \alpha B} \tag{7}$$

For small fields ($\alpha B << 1$), this expression must reduce to equation (5), from which it can be seen that $\beta = e^2 a_B^2/8\mu$, while at high fields ($\alpha B >> 1$), (Eq. 6) is reproduced, hence $\beta/\alpha = e\hbar/2\mu$. However, this expression has no real physical basis and no clear advantages in terms of practical use over the Fock-Darwin or excitonic model, which we will develop below. Indeed, it can be readily shown that the Fock-Darwin expression also reduces to equations 5 and 6 in the appropriate limits. If we restrict ourselves to a single electron–hole pair confined in the dot ($n = l = 0$), equation (4) becomes equation (8):

$$E = E_0 + \hbar\left(\omega_0^2 + \frac{\omega_c^2}{4}\right)^{1/2} = E_0 + \hbar\omega_0\left(1 + \frac{\omega_c^2}{4\omega_0^2}\right)^{1/2} \tag{8}$$

In low magnetic fields ($\omega_c << \omega_0$), we can use the binomial series to expand the term in the square root. Keeping only the first two terms in the expansion gives equation (9):

$$E = E_0 + \hbar\omega_0\left[1 + \frac{\omega_c^2}{8\omega_0^2}\right] \tag{9}$$

Thus, we find that in low magnetic fields, the Fock-Darwin expression yields equation (10):

$$\Delta E = \frac{(\hbar\omega_c)^2}{8\hbar\omega_0} \tag{10}$$

which is clearly proportional to B^2 via the cyclotron energy. Indeed, by substituting equation (3) and $B = \omega_c\mu/e$ into equation (5), we can rewrite it as equation (11):

$$\Delta E = \frac{(\hbar\omega_c)^2}{8(2E_B)} \tag{11}$$

from which we can conclude that $\hbar\omega_0 = 2E_B$. It is trivially seen that in high magnetic field ($\omega_c >> \omega_0$), equation (8) gives an energy shift that is identical to that of equation (6). These results are significant since they demonstrate the underlying physical equivalence of the Fock-Darwin approach to the excitonic approach. This can be understood by remembering that in an exciton, the electron and hole are confined in a harmonic potential that is generated by their Coulomb interaction. Similarly, the enforced wave function overlap of electron and hole in a dot increases the exciton binding energy.

Excitonic model

An alternative approach to the problem has been developed that fundamentally differs from the analyses described above in that, rather than having an extended intermediate field regime between the high- and low-field limits, the system passes directly from one to the other without any discontinuity in $E(B)$ or its derivative (55). Thus, we can write equation (12a):

$$E = E_0 + \frac{e^2 a_B^2 B^2}{8\mu} \text{ for } B \leqslant B_C \tag{12a}$$

and (12b)

$$E = E_0 + E_1 + \frac{\hbar eB}{2\mu} \text{ for } B \geqslant B_C \tag{12b}$$

where E_1 is a constant required for continuity of the equations and B_C is the critical field at which the transition from low- to high-field regime occurs. Imposing the condition of continuity in the derivative at $B = B_C$ gives equation (13):

$$B_C = \frac{2\hbar}{a_B^2 e} \tag{13}$$

When rewritten in terms of the critical magnetic length l_C, we find $l_C = a_B/\sqrt{2}$; i.e., the high-field regime is reached when the magnetic length is $1/\sqrt{2}$ times the zero-field exciton Bohr radius. Having determined B_C, we can now impose the condition of continuity in E at $B = B_C$ and hence determine the constant E_1 as equation (14):

$$E_1 = \frac{e^2 a_B^2 B_c^2}{8\mu} - \frac{\hbar eB_c}{2\mu} \tag{14}$$

After substituting in equation (13) and some simple algebra, this yields equation (15):

$$E_1 = -\frac{\hbar^2}{2\mu a_B^2} \tag{15}$$

This expression is the binding energy of the 3D exciton as defined by equation (3). It should be stressed that it does not actually describe the binding energy of a confined anisotropic exciton. This can be seen by considering the case of the field applied perpendicular to the plane of a quantum well, which in reality, is not very different to the situation for self-assembled QDs where lateral confinement is typically weak compared to vertical confinement. Vertical confinement squeezes the electron and hole wave functions together, increasing their overlap and binding energy. However, compression of the exciton wave-function in the plane is only a by-product of the enhanced Coulomb interaction due to vertical confinement for a 2D system with the addition of much weaker lateral confinement for QDs, making the exciton wave function strongly anisotropic (see section on Electronic coupling of stacked quantum dots below). It is this weak compression of the exciton wave-function in the plane that is probed by the term in equation (15) in a typical experiment when the field is applied in the growth direction; i.e., it does not measure the actual binding energy of the confined exciton but the lateral contribution to that energy. One should expect the size of this energy to be greater, but perhaps not substantially, than the bulk binding energy. Indeed, a lower value than the bulk binding energy might be observed, indicating a spatial separation of electrons and holes in the nanostructure compared with the bulk (see section on Determining the band alignment in quantum dots below). Finally, we return to our problem and obtain equation (16a):

$$E = E_0 + \frac{e^2 a_B^2 B^2}{8\mu} \text{ for } B \leqslant \frac{2\hbar}{ea_B^2} \text{ or } \textit{equivalently}, l_B \geqslant a_B/\sqrt{2}) \tag{16a}$$

and (16b)

$$E = E_0 - \frac{\hbar^2}{2\mu a_B^2} + \frac{\hbar eB}{2\mu} \text{ for } B \geq \frac{2\hbar}{ea_B^2} \text{ or } \textit{equivalently}, l_B \leqslant a_B/\sqrt{2}\,) \tag{16b}$$

This analysis has been successfully applied to high-field PL data for a large number of semiconductor systems such as: InP QDs in $GaInP_2$ (55); InAs QDs in GaAs (56); InAs quantum wires in InP (57); GaSb QDs in GaAs (58,59); InAs QDs in InP (60); GaAs QDs in AlGaAs (38,39); weakly-ordered $GaInP_2$ (61); InP QDs in GaAs (62); Si nanocrystals in SiO_2 (63); and $Ga_{1-x}In_xAs_yN_{1-y}$ quantum wells (64,65). Even though there are two regimes, a set of PL energies as a function of magnetic field can be fit in a single process using the equivalent expression expressed by equation (17a):

$$E = a_1 + a_2 B^2 \text{ for } B \leqslant B_C \tag{17a}$$

and (17b)

$$E = a_1 - a_2 B_C^2 + 2a_2 B_C B \text{ for } B \geq B_C \tag{17b}$$

yielding three parameters: $a_1 = E_0$, B_C, and $a_2 = e^2 a_B^2/8\mu$ (diamagnetic shift coefficient). Further manipulation of these parameters can be applied to determine a_B using equation (13) and $\mu = e\hbar/4a_2 B_C$. It should be noted that when only the ground state recombination is considered using this excitonic approach, the Fock-Darwin formulism or equation (7) results in the same number of parameters which is self-evident since, as we have shown, all three approaches converge in the high- and low-field limits.

Photoluminescence experiments in high magnetic fields

Optics in magnetic fields

Figure 4 shows a schematic diagram of a magneto-PL setup (66) for a pulsed field laboratory (67). Although it looks quite complicated, and indeed timing issues for magneto-PL experiments in

LUMINESCENCE
The Journal of Biological and Chemical Luminescence

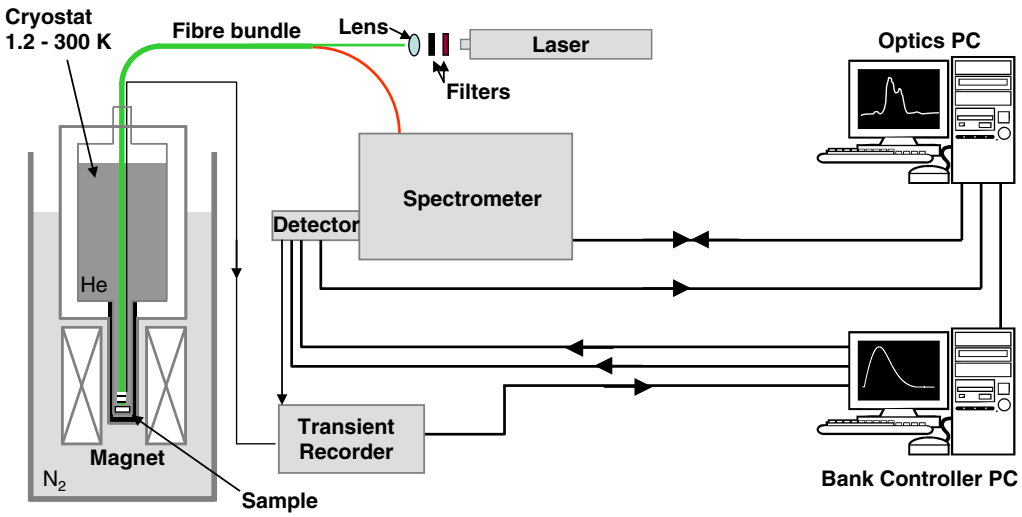

Figure 4. Schematic diagram of a magneto-PL set up for a pulsed field laboratory. For a DC (superconducting) magnet laboratory, the optics are the same but the hardware and connections to control the field and timing for experiments are much simpler, removing the need for two computers. Note that except for the links between the spectrometer/detector and the optics PC, all information is sent via optical link so that the pulsed-field installation is electrically isolated

pulsed fields do need to be quite sophisticated (as we discuss below), the actual optical part is remarkably simple and generic for DC and pulsed magnets. We will only discuss using optical fibres to gain optical access to the sample space in the centre of the magnet; the optics can be far from the magnet (even in a different room), which is a significant practical and safety advantage for pulsed-fields setups where there is a risk of coils exploding. It is also possible to work at much lower light levels before it is necessary to turn the room lights off.

Light from a laser is first passed through a laser interference or band pass filter to remove any unwanted fluorescence lines in the case of a gas laser such as argon-ion or residual laser signal at other wavelengths in the case of diode-pumped solid-state lasers, followed by neutral-density filters to set the order of magnitude of laser excitation power. It is then focused into an optical fibre that carries the laser light to the sample by a microscope objective. Note that this is the only lens in the optics. The laser fibre is typically 200 to 250-μm core multimode high-OH fibre. The lasers used for magneto-PL typically, but not necessarily, emit in the green such that it is not necessary to use more expensive low-OH fibre, while it is essential to use high-OH if exciting in the UV. Output of a tuneable laser in the red or near-infrared may also be used to excite the sample. PL, which is often in the near infrared, is collected from the sample using either a bundle of similar-sized low-OH fibres or a single 500-μm core fibre depending on the detector used. It is important to optically isolate the fibres from each other and from the outside world by using heat-shrink sleeving to reduce fibre fluorescence in the PL collection fibres and avoid the room lights leaking into the fibres. The fibre bundle should be glued without heat-shrink sleeving into a length of metal tube to provide a leak-tight seal at the top of the cryostat. It is also possible to place carefully selected optical components in the cryostat between the fibres and the sample such as a quarter-wave plate plus linear polariser to allow distinction between left- and right-hand circularly polarised light (31). It should be noted that using a multimode fibre produces a spot size on the sample that is ~ 1–2 mm in diameter; larger by an order of magnitude than is typical for PL experiments using an optical cryostat. This has the advantage of allowing more light to be collected for a given laser power density, which is important in pulsed fields where photon integration times are short, but has the disadvantage that it is more difficult to reach high laser excitation power densities. When high excitation power densities are required, a lens can be introduced at the sample end, although in that case, it is difficult to simultaneously match the peak laser power density on the sample with the optimal collection efficiency.

Figure 5 shows different designs for optical fibre bundles to deliver laser light to the sample and collect the luminescence. The choice of fibre bundle depends on the experiment in question, especially the detector. The arrangement in Figure 5a is best suited for a linear InGaAs diode array, such that the core diameter of the collection fibre matches the pixel height, which is typically 500-μm when used in combination with a 1:1 magnification imaging spectrometer. Note that the numerical aperture for spectrometers is smaller than for optical fibres, so not all the light emerging from the fibre can be captured. When using a charge-coupled-device (CCD), it is advantageous to arrange a number of collection fibres in a vertical line in front of the entrance slit of the spectrometer, which illuminates a large area of the CCD, thereby increasing the signal without the need for wide entrance slits (Fig. 5d). At the sample end, the easiest way to arrange a bundle of such fibres is shown in Figure 5b. This is a very efficient arrangement for collecting the PL but has the disadvantage that the laser light is also reflected back up into the collection fibres, which can be problematic in certain cases (see section on Origin of the luminescence from Si nanocrystals below). In such circumstances, an arrangement such as depicted in Figure 5c is preferred.

The magnetic field probes the electronic properties in the plane perpendicular to the direction in which it is applied. Typically and most conveniently, the sample is mounted horizontally in the cryostat with the field applied in the *z* (growth) direction such that the excitonic properties are probed in the plane of the sample (Fig. 6a). This experimental geometry is often called the Faraday geometry. The Voigt geometry shown in Figure 6b requires the sample to be mounted vertically in the cryostat, which is inconvenient. In addition, since the confinement of the wave function in the *z* direction is typically much stronger than in the plane; i.e., the wave function is strongly compressed in the *z* direction, the diamagnetic shift of the PL is, according to

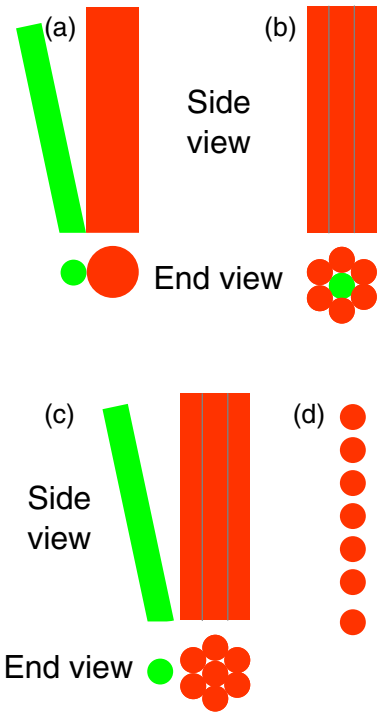

Figure 5. Schematic diagram showing the side and end-on views for different designs of fibre bundles (a) to (c) (sample end), the choice of which depends on the experiment, especially the geometry of the detector. The fibres should be glued into a suitable holder (not shown) to ensure the correct configuration. In (a) and (c), the tilted fibre on the left is the laser excitation fibre (green); in (b), it is the central fibre in the bundle. If a bundle of collection fibres (red) is used, it may be arranged in a line at the spectrometer entrance slit (d)

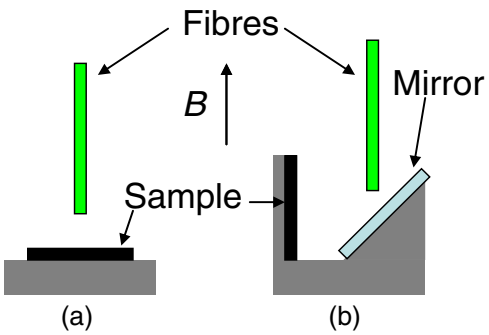

Figure 6. Schematic diagram showing the sample mounted with a magnetic field oriented (a) parallel to the growth direction ($B//z$), also called Faraday geometry and (b), perpendicular to the growth direction ($B\perp z$), also called Voigt geometry. Note that in the latter case, it may also be interesting to consider which crystallographic direction is oriented parallel with the applied field, if for example there is some in-plane anisotropy as is the case with self-assembled quantum wires (57)

equation (5), usually very small. By the same token, it is also very unlikely that the high-field regime will be reached (Eq. 16b), meaning that the effects of Bohr radius and reduced exciton mass cannot be separated. Nevertheless, for certain experiments, it is interesting to probe the extent of the wave function in the z direction (section on Electronic coupling of stacked quantum dots below).

Pulsed magnetic fields

The discussion in the preceding section is applicable to magneto-PL experiments in both DC and pulsed magnetic fields. In the latter case, there are additional considerations due to the transient nature of the field pulse that make the experimental setup considerably more complex. Before discussing this, it is worth stressing that of all experimental techniques considered for implementation in a pulsed field laboratory, PL is one of the most straightforward. There are for example no issues with field-induced voltages in sample wires or microphonic effects associated with the violent nature of the experiment that can plague transport experiments; as far as photons are concerned, there is no difference between DC and pulsed fields. Precautions need to be taken to avoid putting any metal parts on the end of the sample stick; the lower part of sticks used in a pulsed field facility should be made of other materials such as specialised plastics, epoxy resins or ceramics. The only metal is in the wires of the pick-up coil used to measure the magnetic field and those connected to any temperature sensor. Note that the very transient nature of the field implies that it is sufficient to measure the temperature of the sample before the pulse; one need not worry about the temperature sensor's response to the large magnetic field.

The primary disadvantage of pulsed fields is the length of the pulse, which is of the order of a few 10-s to 100-s of ms for a non-destructive coil, depending on the facility, and the long wait between pulses that can vary from a few minutes to several hours depending on the length of the pulse and the peak field; i.e., the energy dissipated. This means that it is essential to take at least one complete spectrum in a pulse requiring the use of multi-channel photon detectors (CCD or linear array). In addition, since it is necessary to have a small field variation while taking data, photon integration times are a few ms at most. Therefore, the PL from samples should be bright and laser power densities should not be low. In practice, this means that most III-V compound semiconductor samples can be studied at low temperatures with laser excitation power densities in the region of 1 Wcm^{-2}. There have also been major advances in detector technology over the last 10–15 years resulting in: (i) substantially faster CCDs, thereby removing the need use an image-intensified CCD (ICCD) to have electronic shuttering (66) which improves both the wavelength range and the quantum efficiency of the detector; (ii) the advent of low-noise liquid-nitrogen or thermoelectrically-cooled InGaAs linear diode arrays that extend the possible wavelength range for PL in pulsed fields up to and beyond the telecoms wavelengths of 1.3 and 1.55 μm; and (iii), the invention of electron-multiplying CCDs (EMCCDs) capable of amplifying the signal of very few photons above the intrinsic electronic noise level of the CDD. The main objective of this subsection is to discuss timing issues related to PL experiments in pulsed fields with particular reference to this new generation of fast and extremely sensitive detectors.

Figure 4 is a schematic diagram of the setup for a PL experiment in pulsed magnetic fields. It looks quite complicated, with many connections between the different pieces of kit and two computers. Two computers are necessary due to the large nature of the infrastructure of such a facility, typically occupying several rooms and because a single central computer is required to control the capacitor bank that serves a number of magnets for reasons of safety. The second issue is that, because of the extreme nature of the experiment in terms of the currents, voltages etc. involved, the exact time of the start of the pulse after pressing the 'fire' button cannot be accurately predicted; as a result, it is necessary to have a sequence of trigger pulses to ensure a successful experiment. Hence, a typical sequence of

LUMINESCENCE
The Journal of Biological and Chemical Luminescence

events is as follows: 1) an arbitrary waveform generator is pre-programmed with one or more trigger pulses to control the point(s) during the pulse at which photons are counted; 2) the voltage on the bank that determines the peak field of the pulse is chosen and the bank is charged; 3) the user presses the 'fire' button; 4) a pre-trigger signal is sent to the detector; 5) after a pause to allow the detector to do any pre-exposure housekeeping, the fire signal is sent to the capacitor bank; 6) the actual start of the pulse is detected via a large voltage spike in the pick-up coil placed close to the sample in the magnet (Fig. 7). This triggers the transient recorder that measures the voltage from the pick-up coil. This signal is later integrated to determine the magnetic field. The transient recorder also sends a trigger to the arbitrary waveform generator; 7) the arbitrary waveform generator sends the pre-programmed trigger pulse(s) to the detector; and 8), the detector sends a pulse or series of pluses for multiple exposures back to the transient recorder so that the actual shutter sequence can be recorded. Note that the exact details of this sequence depends on the detector and the number of spectra to be taken; i.e., PL intensity. If a linear array is used, then it is necessary to read each spectrum immediately after counting the photons during the pulse, which typically introduces a minimum delay of 0.5 ms between spectra. For a CCD, which is a 2D array, readout is slow, so this must be done when the experiment is finished. Furthermore, unlike the InGaAs linear diode array, a CCD cannot be switched off, so it is necessary to vertically shift the charge in the rows very quickly by use of a fast CCD.

With a sophisticated sequence of control signals such as the one described above, it is possible to accurately design a sequence of exposures to extract the maximum possible amount of data out of each pulse and therefore make the experiment very efficient. An example of this is shown in Figure 7 for a series of 17 0.5-ms exposures using an InGaAs linear diode array with a readout time of 0.5 ms. A complete experiment would consist of a few pulses with different peak fields (bank voltages) to get good coverage of the whole field range from 0 to 50 T.

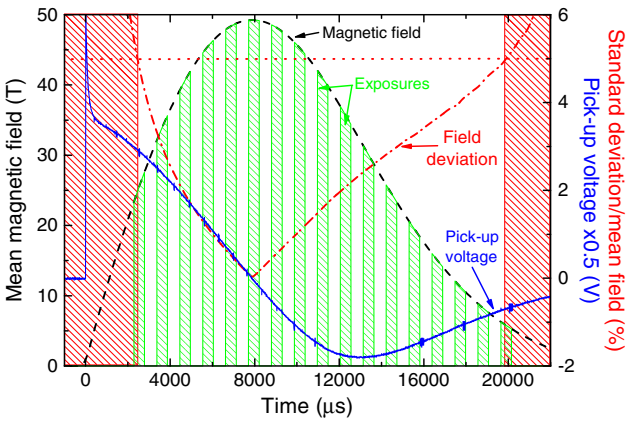

Figure 7. Shutter sequence for 0.5-ms exposures (green hashed areas in the central part of the figure) at 17 different field values for an InGaAs linear array with 0.5-ms readout time as detector. The solid line (blue curve) is the voltage from the pick up coil from which the magnetic field is determined. In this figure, the magnetic field shown (black dashed line) is the mean value at any given point averaged over a period of 0.5 ms (the exposure time). The dot-dashed line (red) is the standard deviation in field over the 0.5-ms period divided by the mean field. This plot thus specifies the percent deviation in field for a given exposure time. Choosing boundaries for an acceptable level of field deviation for the exposures during the pulse, 5% in this case (indicated by the red horizontal dotted line), defines the number of spectra that can be acquired

With a shorter exposure time, more spectra can be taken, but even in the limit of zero exposure time, a maximum of 50 spectra can be taken with the InGaAs detector in a 25-ms pulse like the one in Figure 7. This is not the case for a CCD, where it is possible to take a large number of spectra by reducing the exposure time and number of rows of the CCD that are illuminated. Figure 8 shows a colour contour plot for a series of 127 spectra taken by illuminating 8 rows of a frame transfer CCD and count time of 200 μs/spectrum. Under such conditions, the disadvantage of short photon integration times becomes a significant advantage; an entire experiment in 25 ms.

Illustrative examples

In this section, we illustrate the previous discussion of the theory and experimental techniques with four examples from four different materials systems. The examples are chosen to demonstrate how magneto-PL can be used to elucidate different physical phenomena in semiconductor nanostructures such as: band offsets in QDs; electronic coupling of stacked QDs; the origin of PL from nanocrystals; and novel effects in type-II QDs. Further details of these investigations can be found in the relevant references. Besides these, there are numerous other phenomena and a vast body of work on for example, GaAs quantum wells, self-assembled QDs, and II-VI nanoparticles that are so large that it is impossible to discuss them in this review. Many of them have already been discussed in previous reviews or book-length studies (8,68).

Determining the band alignment in quantum dots

After the energy gap, the value of the conduction band minimum with respect to a clearly defined zero of energy (vacuum level) is an important parameter for any semiconductor. According to Anderson's rule, this quantity, called the electron affinity χ, allows the positioning of the conduction band minima and eventually the valence band maxima of different semiconductors on the same energy scale (30). The nature of the band alignment at the interface of two semiconductors forming a heterojunction is a determining factor for the electronic and optical properties of heterostructure devices, and thus is of crucial importance.

Figure 9 shows two of the many possibilities that can occur when a few monolayers of material B are sandwiched between other materials. Depending on the sign of the conduction and the valence band offsets at the interface, it is easily appreciated that only under particular circumstances will both electrons and holes be confined within the thin layer of material B. This situation is depicted in Figure 9a and corresponds to what is called a type-I or straddling band alignment. Alternatively, the situation depicted in Figure 9c might also occur, where only one type of carrier (electrons in Fig. 9c, but it could be holes) will be confined in the thin layer of the material C, whereas the other type will be repelled away from it. This is called type-II or staggered band alignment.

While in the case of simple heterojunctions and quantum wells, there exists well-established electrical characterization methods to determine the type of band alignment, and indeed the relative alignment between most pairs of commonly used semiconductor materials is now known to high precision, for QDs this is not always easy. This is because the process of self-assembly responsible for the formation of QDs through the Stranski-Krastanow growth route involves a complex interplay of strain relaxation and a high probability of alloying due to inter-diffusion of material across the interface. These effects affect the position of the

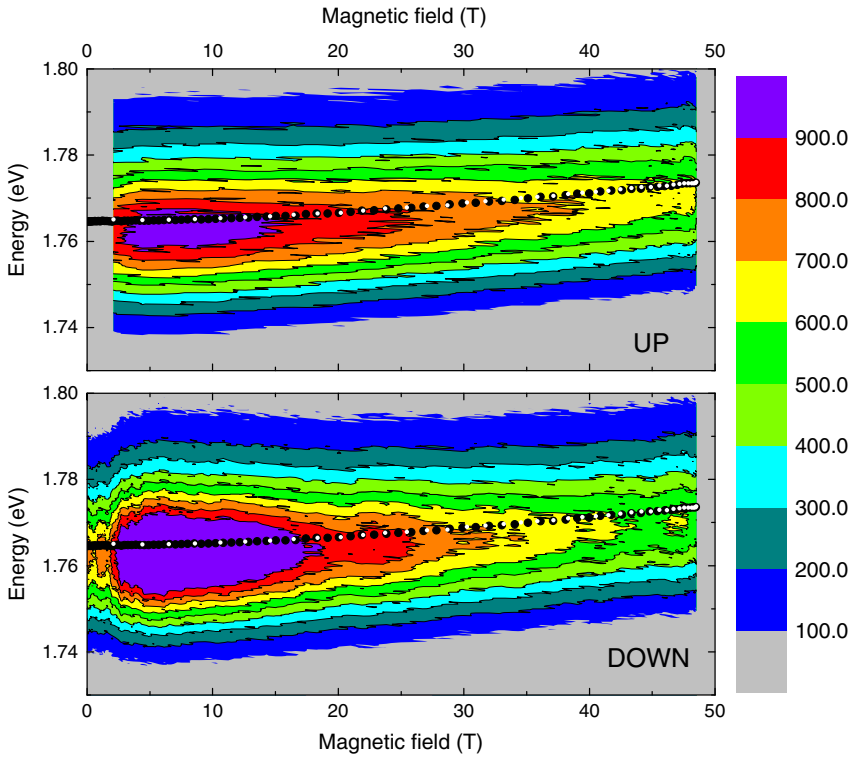

Figure 8. Colour contour plot of PL from InP/GaInP$_2$ self-assembled QDs as a function of magnetic field. The entire dataset of 127 spectra was taken in a single 25-ms pulse by illuminating just 8 rows of a frame transfer EMCCD with 512 columns (total of 65,024 data points). The laser power was 100 mW, temperature 2.2 K, and integration time 200 μs. The upper panel shows spectra taken with the field sweeping up and the lower panel with the field sweeping down. The white and black dots represent the centre of mass of the peak for the up and down sweeps, respectively. These are offset from the intensity maxima due to an asymmetry in the peak. The data were taken at 2.2 K in a superfluid He bath cryostat to minimise noise from bubbles. This source of noise can be observed in the modulation of the intensity of the down data as a result of heating from the magnetic field pulse. Nevertheless, as can be seen from the excellent correspondence of the black and white dots, the centre of mass was unaffected

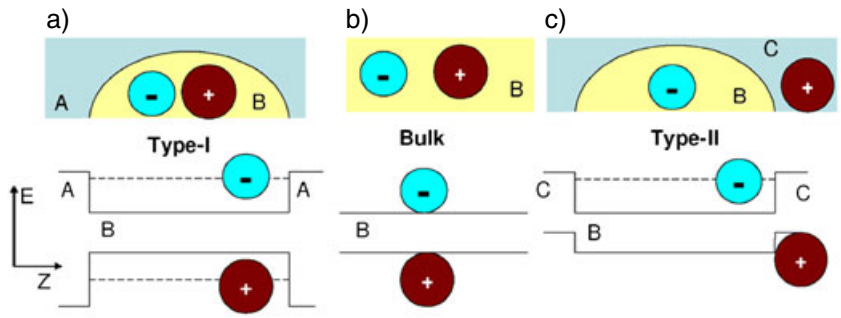

Figure 9. Schematic depiction of an exciton in bulk material (b) and QDs with type-I and type-II band alignment. Material combination B/A (a) has type-I alignment (e.g., InAs/InP and possibly InP/GaInP$_2$), whereas B/C (c) has type-II band alignment (e.g., InP/GaAs). Type-I confinement results in a decrease in the exciton radius and an increase in the exciton binding energy. For QDs with type-II band alignment, the exciton binding should be weaker and the radius larger compared to the bulk values, while the emission energy can be smaller than the band gaps of either of the two materials

conduction and valence band levels in the QD and, hence, it is not easy to predict the value of the band offsets even if the positions of the conduction band minima and valence band maxima are well established for the corresponding bulk materials.

If material B is InP, then material A in Figure 9a might be GaInP$_2$ and material C in Figure 9c might be GaAs. Specifically for InP QDs in GaAs, it was theoretically predicted that they confine neither electrons nor holes (69), whereas experimental reports assumed a type-II band alignment (70). It is obvious from Figure 9 that the exciton size and binding energy in the same material (InP) will be a strong function of the heterostructure boundary conditions. In type-I QDs, excitons will be squeezed to a size smaller than their bulk value whereas in type-II systems, the excitons will be larger since the electron and hole are spatially separated by the staggered band alignment. Hence, magneto-PL is an excellent technique to settle the issue of band alignment (62).

Figure 10 demonstrates how the discussion on analytical models is put into practice and how magneto-PL data can be used to find the exciton size. The data (blue circles) show the field-dependence of the PL peak energy for InP/GaAs QDs grown by metal-organic vapour-phase epitaxy (71). The solid line is a fit to equation 16, while the dotted and dashed lines

LUMINESCENCE
The Journal of Biological and Chemical Luminescence

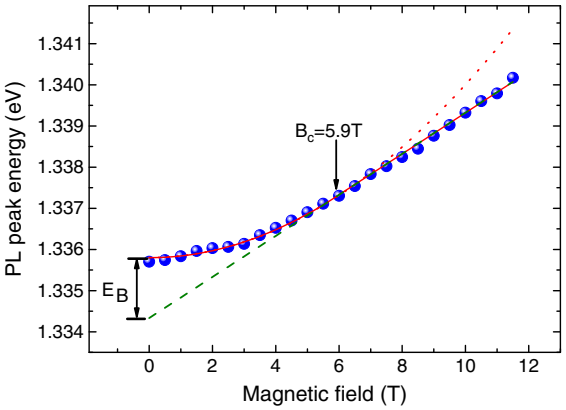

Figure 10. Field dependence of PL peak energy of InP/GaAs quantum dots measured at 4.2 K (blue circles). The solid line is a fit to Equation (16), while the dotted line is the continuation of the low field portion (Eq. 16a) to high field and the dashed line is a continuation of the high field portion (Eq. 16b) to low field. The crossover from Coulombic to magnetic confinement occurs at 5.9 T and corresponded to an effective Bohr radius of 15 nm. The extrapolation of the linear slope measured at high field to zero field gives a binding energy of 1.5 meV

show continuations of the parabolic low-field fit (Eq. 16a) to high field and the linear high-field fit (Eq. 16b) to low field, respectively. This figure demonstrates that the excitonic model developed earlier provides a good description of what is observed in experimental data and is entirely typical. The crossover between the two regimes is well-defined in the exciton model and directly gives the exciton size in the plane perpendicular to the applied field; 15 nm in this case. The difference between the zero-field PL peak energy and the extrapolation of the high-field linear dependence to zero field gives the corresponding binding energy. Table 1 compares these values with those for excitons in bulk InP and type-I InP/GaInP$_2$ QDs. It can be seen that all parameters (diamagnetic shift, Bohr radius, and binding energy) show that the excitonic binding is weakest for InP/GaAs QDs and even weaker than in bulk InP. This can only be the result of spatial separation of electron–hole pairs, leading to the conclusion that InP/GaAs QDs have type-II band alignment.

Table 1. Comparison of exciton parameters in InP under different boundary conditions. An experimental value for the binding energy in InP/GaInP$_2$ was not available since insufficiently high magnetic fields were applied to reach the high-field regime, but given the tiny diamagnetic shift, it is likely to be substantially larger than in the other cases

	Diamagnetic shift (eVT^{-2})	Bohr radius (nm)	Binding energy (meV)
InP/GaAs QDs	42.4 ± 0.5	15.0 ± 0.1	1.5 ± 0.1
Bulk InP	40[a]	~ 12[b]	4.8 ± 0.2[c]
InP/GaInP$_2$	2-5[d]	2.7-4.3[b]	—

[a]de Godoy MPF, Nakaema MKK, Iikawa F, Carvalho W, Ribeiro E, Gobbi AL. Biaxial stress ring applications to magneto-optical studies of semiconductor films. Rev Sci Instrum 2004;75:1947–51.
[b]Estimated from the diamagnetic shift using 0.08 m_0.
[c]Nam SB, Reynolds DC, Litton CW, Collins TC, Dean PJ, Clarke RC. Free-exciton energy spectrum in InP in a magnetic field. Phys Rev B 1976;13:1643–48.
[d](55) and Sugisaki M, Ren H-W, Nair SV, Nishi K, Masumoto Y. External-field effects on the optical spectra of self-assembled InP quantum dots. Phys Rev B 2002;66:235309.

Electronic coupling of stacked quantum dots

Self-assembled QDs are spontaneously formed with areal number densities of ~ 10^{10} cm^{-2} in a strain-driven process when a few monolayers of a semiconductor material are deposited on the surface of a semiconductor with a different and typically smaller lattice constant (72). InAs on GaAs is easily the most common example. Subsequently, the dots should be capped with more of the substrate material to study their optical and electronic properties or to incorporate them in a device. It is also possible to grow stacked layers of QDs and, if the capping layer is not too thick, vertically aligned dots (73). This vertical alignment is also a strain-driven effect: tensile strain of the capping layer due to the underlying dots generates preferential sites for the formation of dots in the upper layer (74). If the intervening capping layer is sufficiently thin, then the dots could become electronically coupled due to quantum-mechanical tunnelling of the wave function through the potential barrier caused by the cap. Such a system can be described as a quantum dot molecule (75). Electronic coupling of quantum-dot bilayers or multiply stacked layers is not only an interesting tuneable physical system but has a number of applications in, for example, quantum information processing (76), generating highly-efficient intermediate-band solar cells (77) using 3D arrays of electronically coupled QDs, providing a seed layer for growth of dots for narrowing the inhomogeneous broadening and generating long-wavelength emission (78) and improving the performance of QD lasers (79,80).

The question is therefore: how can we know if vertically-aligned pairs or stacked dots are electronically coupled? Magneto-PL can provide a definitive answer (81). Since it directly probes the extent of the exciton wave function and self-assembled QDs are typically very flat; i.e., carriers are strongly confined in the growth direction (dots are typically a few nm's high) and much less confined in the plane of the sample (dots are typically a few tens of nm's in diameter), electronic coupling will increase the extent of the wave function in the growth direction by several hundred percent. This can be investigated by applying the magnetic field perpendicular to the growth direction in the plane of the sample (Voigt geometry). Figure 11 shows zero-field PL spectra for a single layer (sample A) and a series of ten-fold stacked layers of InAs/GaAs QDs with interlayer distances of 9.8, 5.5 and 3.1 nm (samples B, C and D, respectively). The samples were grown by molecular beam epitaxy at the University of Nottingham. It can be seen that there is a systematic trend of lower PL energy going from the single layer sample to the stacked layer samples with reduced layer separation. In particular, there is a large decrease in PL energy (~ 79 meV) when going from an interlayer separation of 9.8 to 5.5 nm. This might be taken as evidence for the onset of electronic coupling but is certainly not proof. The redshift may equally be the result of strain relaxation (82,83). Indeed, there is a significant redshift of an additional 40 meV as the interlayer distance is reduced by only 2.4 nm between samples C and D. It is difficult to explain both shifts exclusively in terms of the onset of electronic coupling. In fact, it has been shown that either a red or blue shift (83,84) can be

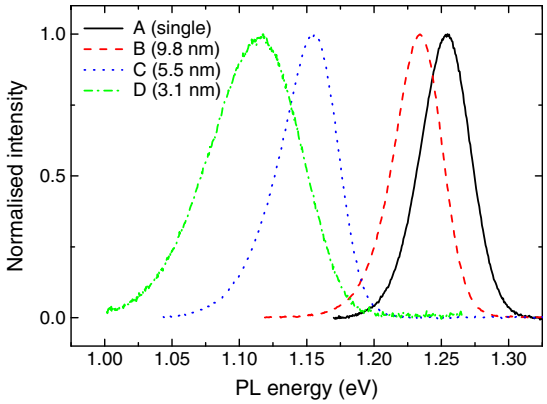

Figure 11. Zero-field PL spectra for a series of InAs/GaAs QD samples. Sample A has a single layer of dots whereas samples B to D have 10 stacked layers of dots (layer separation is given in brackets). A systematic decrease of the photoluminescence energy with decreasing layer separation is observed

observed when decreasing the layer separation of stacked dots and that PL energy is affected by electronic coupling, strain, indium segregation and Coulomb interaction (85), or by an increase in size as a by-product of the stacking (86).

With this in mind, we now turn to the magneto-PL. Figure 12a shows the PL energy with the field applied parallel to the growth direction *z* (*B*//*z*, Faraday geometry). The result seems rather uninteresting; besides the change in the zero-field PL energy, the data for samples A to C seem almost indistinguishable. Indeed, the total size of the shift between zero and 50 T was 18.9, 18.7 and 18.2 meV for samples A, B and C, respectively. Only sample D was different, with a substantially increased shift of 28.8 meV over the whole field range. This change was the result of a smaller reduced mass for the exciton, which can be inferred from the increased gradient at high fields (see Eq. 6) brought about by a

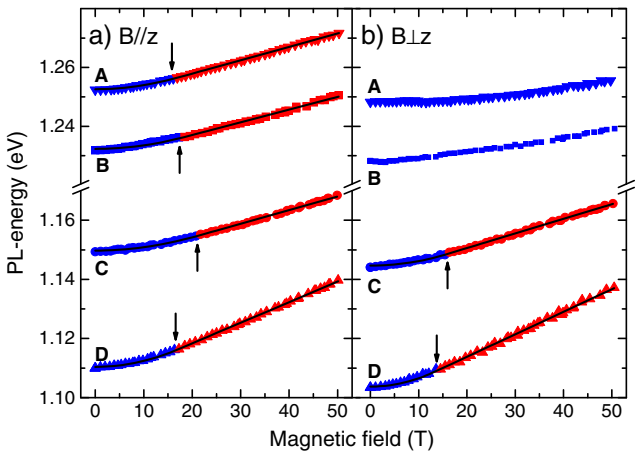

Figure 12. Magneto-PL data for the samples in Fig. 11 with magnetic field applied (a) parallel to the growth direction (*B*//*z*) and (b) perpendicular to the growth direction (*B*⊥*z*). The symbols are the experimental points and the solid lines are fits to Equation (16). The arrows mark the transition from the low-field regime (blue data) where the PL energy has a parabolic dependence on magnetic field to the high-field regime (red data). There seems to be little change in the data for the different samples with *B*//*z*, but a striking change in *B*⊥*z* data as we go from sample B (9.8 nm layer separation) to sample C (5.1 nm layer separation). For samples A and B and *B*⊥*z*, the data is parabolic to the very highest fields, indicating that the exciton wave function was strongly compressed in the growth direction due to the flat geometry of the dots. For samples C and D, the high-field regime was reached at very low fields, demonstrating a massive expansion in the vertical extent of the wave function due to electronic coupling

reduction in the strain in the dots (81,82). More interesting is the equivalent data with the field applied in the plane of the sample (*B*⊥*z*, Voigt geometry) shown in Figure 12b. The field-induced shift for samples A and B are very similar to each other but remarkably different from that in Figure 12a, being about 50% smaller. More significant is that the data is parabolic in *B* over the entire field range, meaning that the high-field regime is not reached. As mentioned above, this is quite normal for a single layer of self-assembled QDs due to their typically very flat geometry. We therefore conclude that the exciton wave functions of the dots in sample B are similarly compressed in the growth direction, and that for interlayer separations of 9.8 nm the dots are not electronically coupled. The behaviour of samples C and D are quite different. With *B*//*z* the magneto-PL data for samples B and C are almost indistinguishable, whereas the total shift for sample C with *B*⊥*z* is almost double that of sample B. The *B*⊥*z* data for samples C and D is very similar to *B*//*z;* the shift is relatively large and there is clearly a high-field regime where the shift is linear with *B*. This is direct proof of a large increase in the vertical extent of the exciton wave function as a result of electronic coupling.

Origin of the luminescence from Si nanocrystals

P. Ball (87) stated that 'The information age suffers from a split personality'. While Si is the basis for the processors and memories used in the microelectronics industry, its indirect band-gap makes it an intrinsically poor emitter. For this reason, the photonics industry relies on III-V compound semiconductors that have a direct band gap to make lasers and light-emitting diodes. This incompatibility between the partners of information and communication technology is an issue that is becoming even more pressing with the desire to bring low-cost ultrafast optical broadband to the home and push datacoms into the Tbs^{-1} range, thereby applying significant pressure to co-integrate electronic and photonic function at chip level. Thus, the observation of visible luminescence at room temperature from porous Si in 1990 generated a considerable amount of interest (88,89). Although the thrust of the research has now moved to the study of Si nanocrystals embedded in an SiO_2 matrix (90), in the two decades since the initial discovery, a debate has raged about the microscopic origin of the luminescence (91): is it a result of quantum confinement (QC) in nanocrystalline Si (92–94) or is it due to optically active defect states at the Si/SiO_2 interface? Clearly, it has been difficult to distinguish between the two mechanisms. Decreasing the size of a nanocrystal will not only change the energy of quantum confined states but also increases the surface to volume ratio, and it believed that the interface states are influenced by nanocrystal size (95,96) following the band gap widening, for example (97).

It was recently shown that a large magnetic field can be used to unambiguously distinguish between the two mechanisms (63). The idea behind the experiment is similar to that presented in the previous section; i.e., using the field to test if the extent of wave function under investigation is large or small. Here, however, large (corresponding to QC) means just a few nm's and small (corresponding to a defect state) means < than 1 nm. In practice, this means detecting a diamagnetic shift that is somewhere between almost nothing (~ 1 meV) and nothing. This is made worse by the fact that: i) the PL peak is extremely broad, with a full-width at half-maximum of 300 meV; ii) the PL from Si nanocrystals is extremely weak compared to III-V semiconductors; and iii), it coincides with the fluorescence signal from the optical

LUMINESCENCE
The Journal of Biological and Chemical Luminescence

fibres (Fig. 13), which is particularly strong for this experiment because it is necessary to excite the sample with UV. Developing measures to counteract these challenges took considerable effort. Eventually, those chosen were the purchase of a highly-sensitive EMCCD camera, inserting a break in the laser fibre just above the top of the cryostat so that a UV band-pass filter could be inserted to reduce the fibre fluorescence signal, and mounting the sample at an angle of 8° (Fig. 13). This was used in combination with the fibre bundle design shown in Figure 5c and arranged so that the angles added to minimise back-reflection of laser light into the seven collection fibres. In addition, since PL was weak, it was only possible to take data at the peak of the field pulse with a photon integration time of 5 ms; i.e., one field data point per pulse. To counteract the effects of thermal drift for such an extended experiment and any issues with mechanical realignment due to the violent nature of the experiment, the diamagnetic shift was defined as the difference between the centre of mass of the PL as measured for each field pulse and the average centre of mass of PL spectra taken before and after each pulse.

Figure 14 shows the field dependence of the centre of mass of the PL from Si nanocrystals in SiO_2 produced by Zacharias *et al.* (98) (now at Helmholtz-Zentrum Dresden-Rossendorf) via the decomposition of a SiO/SiO_2 superlattice by high-temperature annealing. Figure 14a shows data for an as-annealed sample. There is no clear diamagnetic shift, which leads us to conclude that the origin of the PL is defect related. The presence of defects in the sample was also directly verified using electron spin resonance (ESR). Note that although none of the defects identified by ESR were PL-active, this does not exclude the presence of PL-active defects. The next step was to passivate the sample with hydrogen to remove the defects, as verified by ESR. The effect of this on the magneto-PL was remarkable. Figure 14b shows that the passivated sample had a very clear diamagnetic shift consistent with a parabolic field dependence and QC as the origin for the PL. By assuming a reduced exciton mass of 0.2 m_0, a wave function extent in the plane of the sample of 4.9 ± 0.1 nm was extracted. It should be noted that this was significantly $>$ the 3 nm diameter of the nanocrystals determined by high-resolution transmission electron microscopy (63), a difference that can be attributed to leaking of the wave function through a sub-oxide layer (99). In the final stage, the sample was irradiated with UV to re-introduce the defects via the Stæbler-Wronksi effect (100), again verified by ESR. The result of this treatment on the magneto-PL is shown in Figure 14c: the diamagnetic shift disappeared and defects were the origin of the PL again. Hence, besides showing that magneto-PL can distinguish between the two mechanisms, it also demonstrated that both can give rise to PL, that the defect-related mechanism dominates, and that it is possible to switch between the two at will in a single sample. The same idea was subsequently used to establish that the emission from InN (another promising

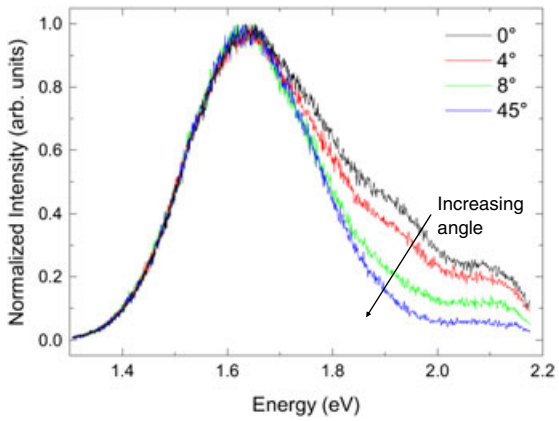

Figure 13. Zero-field PL from Si nanocrystals in a SiO_2 matrix. The high energy tail is the result of fluorescence from the optical fibre and can be reduced by a series of measures, for example by mounting the sample at an angle so that the UV laser excitation light is not reflected into the collection fibres

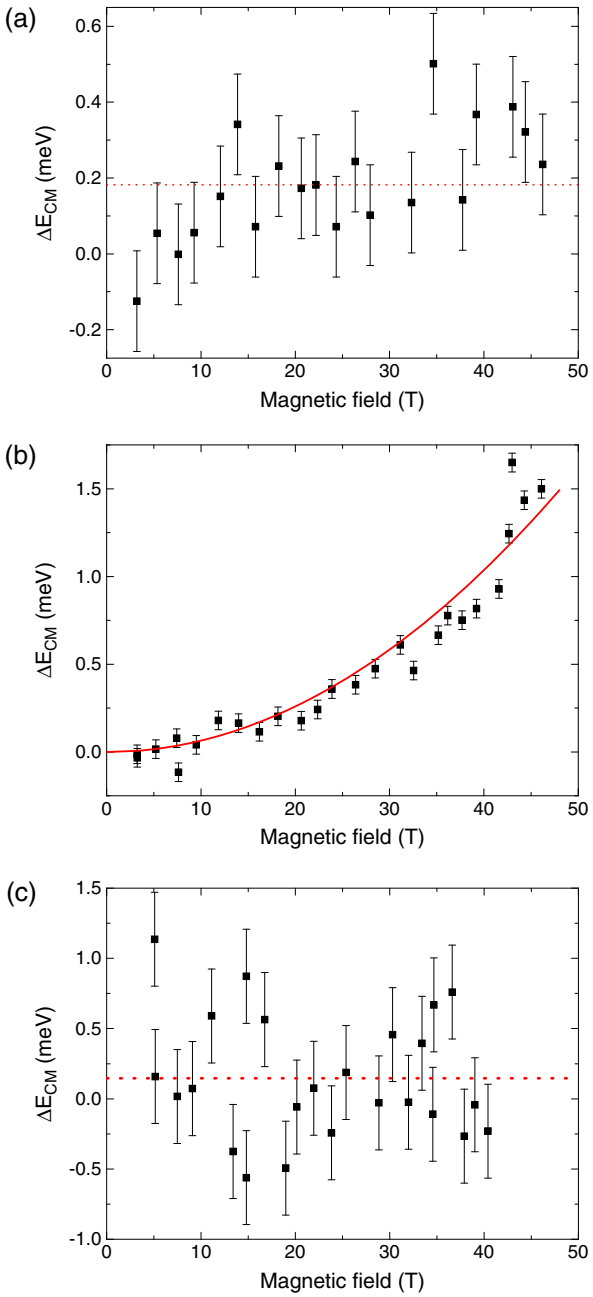

Figure 14. Shift of the centre of mass of PL (ΔE_{CM}) from a Si/SiO_2 nanocrystal sample as a function of magnetic field. The error bars are the mean of the absolute difference in the centre of zero-field spectra taken before and after each pulse. (a) As-annealed sample, (b) after passivation with H, and (c) after subsequent irradiation with UV. The dotted lines in (a) and (c) are the average PL energy over the entire field range, while the solid line in (b) is a fit to Equation (5)

material) was primarily defect related since the measured diamagnetic shift was smaller than that expected from conventional excitons (101).

Excitonic Mott transition in type-II GaSb/GaAs quantum dots

The final example is GaSb/GaAs QDs. In common with InP/GaAs QDs discussed above, it is a type-II system, although of the opposite kind; i.e., the holes are confined and the electrons are free (102). GaSb/GaAs has been much more intensively investigated than InP/GaAs due to its deep confining potential for holes (58) and resulting potential applications in memories (103), lasers (104) and solar cells (105). There have also been a number of investigations of GaSb/GaAs QDs in high magnetic fields (58,106,107), but here we concentrate on a particular set of experiments that not only used high magnetic fields to probe the nature of excitonic state but also to modify that state, demonstrating the observation of Mott transitions.

The sample, which consisted of a single layer of GaSb QDs in a GaAs matrix, was grown by metal-organic chemical vapour deposition at the Technical University of Berlin. Figure 15 shows the zero-field PL at different laser excitation power densities and a temperature of 15 K. It can be seen that as the laser power increased, the QD peak at ~ 1.1 eV at low power blueshifted and broadened such that it started to merge with the more intense wetting layer peak. The blueshift is characteristic of type-II systems and is the result of a combination of band-bending (108) due to charge separation and capacitive charging (109,110). We concentrate, however, on the broadening, which is indicative of a Mott transition (111) from a localised excitonic state where the unconfined electrons are bound by the Coulomb interaction to holes confined in the dots (58) to a metallic state, where a high photo-excited electron density screens the electrons from the positively charged dots forming a one-component plasma. Support for this assertion comes from the inset in Figure 15 that compares low-power QD PL peak at low and high temperatures and high field. No change in linewidth was observed, demonstrating that the broadening observed in the main part of the figure was not the result of heating due to the high laser-excitation power.

Proof that this was the case is provided by measurements in high magnetic fields. Figure 16 shows the exciton binding energy and radius, as determined by fitting the magneto-PL data to Eq (16). It can be seen that as the laser power increased, there was a decrease in the binding energy and a corresponding increase in the exciton radius, both of which are features of a steady reduction in the strength of the binding between electrons and holes. It should be noted that such an effect is completely excluded in type-I QDs where electrons and holes are co-located in the same small volume, although observation of a Mott transition was reported in type-I quantum wires (112).

Figure 17 shows how a high magnetic field can also be used to actually modify the physics of the system as well as probe it. The left-hand panel shows the PL energy as a function of magnetic field for different laser powers. At low laser power (Fig. 17c), the magneto-PL data followed the usual parabolic and then linear field-dependence expected for excitonic behaviour. At high laser power (Fig. 17a), the PL energy increased linearly with field at low laser power, indicative of free electrons; i.e., a metallic state, but at ~ 15 T, there was an unexpected change and the field dependence became parabolic. This is attributed to a field-induced Mott transition in which the magnetic field reduces the wave function extent of the electrons in the plasma, such that they feel the localising potential of the holes that are confined to the QDs; i.e., it reduces the screening and magneto-excitons are formed, effectively diluting the system (32). The relationship between the two forms of Mott transitions are illustrated in Figure 17d, which shows the QD PL line-width as a function of *B* for different laser powers. Equating a broad PL line to a metallic state and a narrow line to an insulating state, Figure 17d can be viewed as a metal-insulator phase diagram for this system. At low laser power (0.2 Wcm^{-2}), PL line-width was always narrow, indicating an excitonic insulating state. At high power (10 Wcm^{-2}) and zero or low magnetic field, the line was broad (metallic state) but as *B* is increased, electrons became increasingly localised, the

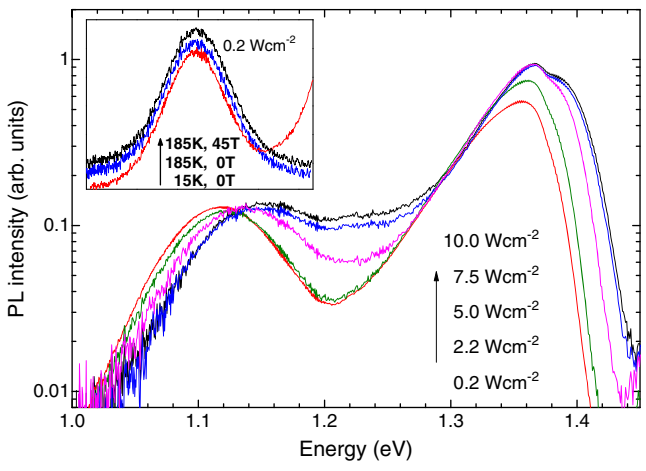

Figure 15. Low temperature (15 K) zero-field PL from a GaSb/GaAs QD sample for different incident laser excitation powers. The low- and high-energy peaks are from the QDs and wetting layers, respectively. As the laser power was increased, both peaks blueshifted; a characteristic feature of type-II systems. The QD PL peak also broadened substantially; evidence for a carrier-density-driven Mott transition from an excitonic (insulator) state to a free-electron (metallic) state. The inset compares the QD low-excitation-power PL peak under different conditions. Neither high temperature nor high magnetic fields had any effect on linewidth

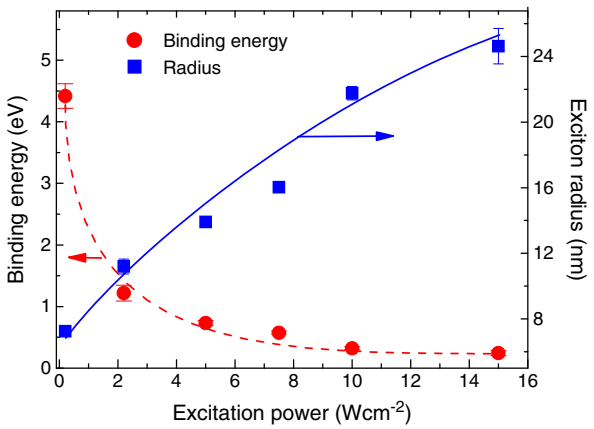

Figure 16. In-plane contribution to the binding energy (circles) and Bohr radius (squares) as determined from the excitonic analysis described above for GaSb/GaAs QDs as a function of laser power (data taken at 4.2 K). The lines are guides to the eye. As the laser power is increased there is a dramatic increase in the exciton radius and corresponding decrease in binding energy. Both are symptomatic of a weakening of the Coulomb attraction between electrons and confined holes, leading to a transition from localised electrons (insulator) to free electrons (metal)

LUMINESCENCE
The Journal of Biological and Chemical Luminescence

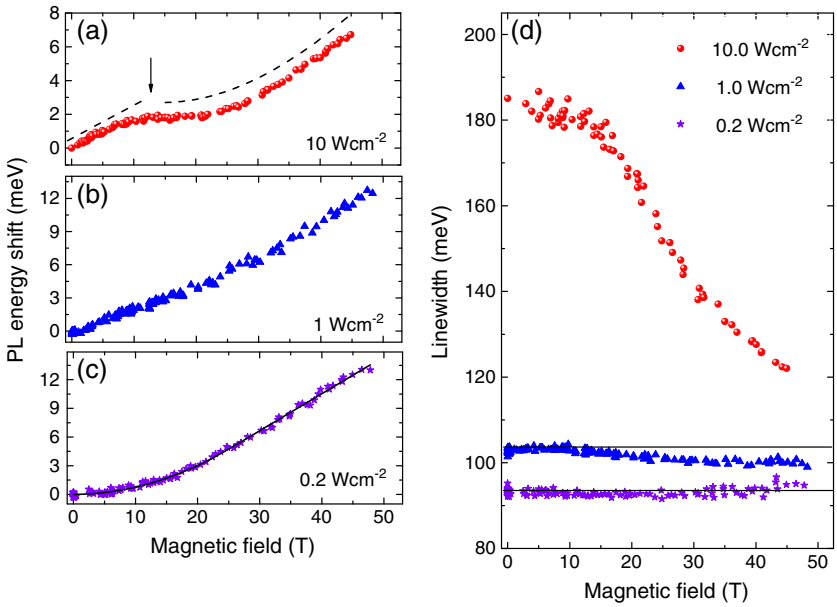

Figure 17. (a) to (c); PL peak energy shift for GaSb/GaAs QDs as a function of magnetic field for different incident laser powers at 15 K. At 0.2 W (c), the data shows the usual low-*B* parabolic and high-*B* linear dependence. At a laser power of 1 Wcm^{-2}, the data begins to deviate from this typical behaviour. By 10 Wcm^{-2}, the reverse of the normal field dependence is observed. The low-field portion of the data is linear with *B*, which is characteristic of free carriers (metallic state), then, at ~ 15 T, there is a kink in the data and the curve follows a parabolic dependence characteristic of bound carriers (insulator). Further evidence that this is a magnetic-field-induced metal-to-insulator Mott transition is given in (d), which shows the line width of the QD PL as a function of field for different laser powers at 15 K. At low laser power (0.2 Wcm^{-2}), the PL was (relatively) narrow and field independent. At 1 Wcm^{-2}, the line width was slightly enhanced and showed a slightly decreasing trend increasing field. At 10 Wcm^{-2}, the line width was strongly enhanced indicative of a metallic state but showed a dramatic decrease as an increasingly large magnetic field was applied

line width decreased, and the system again headed towards the insulating state.

In closing, we make two further interesting observations. The first is that it was previously reported that increasing laser power increases the binding of electrons (58) to GaSb/GaAs QDs; i.e., the exact opposite of what we described here. This apparent contradiction was resolved in a recent study where both effects were observed in two slightly different samples and can be explained by subtle differences in the relative strengths of the electron–electron (screening) and electron–hole interactions (106). In samples where the morphology allows the electrons to get close to GaSb nanostructures, the electron–hole interaction dominates and increasing in the photo-excited carrier density by turning up the laser power results in more-strongly-bound excitons. On the other hand, where the carriers were repelled from the dots, for example by strain in the surrounding GaAs (58), the electron–electron interaction (screening) dominates and increasing the laser power weakens the excitonic binding. The second observation is that we showed that the application of a magnetic field can actually modify rather than just probe the system. This was also seen in magneto-PL experiments of InAs/GaAs QDs (113) where it was shown that at temperatures above 100 K, the application of a magnetic field noticeably increased the effective confining potential of the dots but in a way that depended on dot size, weighting the response of the PL to magnetic field increasingly towards that of smaller dots as the temperature was increased. In such situations, interpretation of magneto-PL data needs to be approached with care. Generally, we expect the application of a magnetic field to change the exciton binding energy. This effect will be small when both electrons and holes are strongly confined, but it is not explicitly included in any of the analytical descriptions of the PL from QDs in high magnetic fields.

Conclusions

Photoluminescence in high magnetic fields is a versatile and powerful tool for the investigation of semiconductor nanostructures in a very wide range of materials systems. It can reveal insights into the nature of confinement and the interaction between confined carriers that cannot be gained using other techniques. A rigorous treatment of the physics behind such experiments is a largely intractable problem that requires sophisticated numerical approaches that also take into account the detailed morphology of the samples under investigation, including effects of shape, composition and strain, as well as the complex physics of bound electron hole pairs in magnetic fields. Such approaches have thus only been used in a few cases. However, the majority of experiments are performed on large ensembles of quantum dots probing the average response, and approximate analytical analyses of such data are thus able to reveal the key physics, principally based on the notion that the magnetic field provides a length scale to probe the exciton wave-function extent, the latter of which may be determined by spatial confinement, the Coulomb interaction, or a combination of the two.

Acknowledgements

We would like to thank all of our many co-workers and colleagues who contributed to this research. Particular thanks go to Fritz Herlach and Johan Vanacken, who setup and continue to maintain the pulsed high magnetic field laboratory at the KU Leuven and to Victor Moshchalkov, the group head. We are very appreciative of the commitment and enthusiasm of many students and postdocs, especially Rik Provoost, Tony Vanhoucke, Jochen Maes, Stefanie Godefroo, Thomas Nuytten and Mazliana Ahmad Kamarudin, who undertook much of the experimental

work. The research would also not have been possible without many very supportive international collaborators, notably Francois Peeters, Dieter Bimberg, Martin Geller, Andrei Schliwa, Karl Eberl, Arnab Bhattacharya, BM Arora, Mohamed Henini, Laurence Eaves, Andre Stesmans and Margit Zacharias.

References

1. Von Klitzing K, Dorda G, Pepper M. New method for high-accuracy determination of the fine structure constant based on quantized Hall resistance. Phys Rev Lett 1980;45:494–7.
2. Tsui DC, Stormer HL, Gossard AC. Two-dimensional transport in the extreme quantum limit. Phys Rev Lett 1982;48:1559–62.
3. Arakawa Y, Sakaki H. Multidimensional quantum well laser and temperature dependence of its threshold current. Appl Phys Lett 1982;40:939–41.
4. Klingshirn CF. *Semiconductor optics (3 rd edition)*. Berlin: Springer-Verlag, 2006
5. Landau LD, Lifshitz EM. *Quantum mechanics: non-relativistic theory, Volume 3 (3rd edition)*. Oxford: Pergamon Press, 1981.
6. Ashcroft NW, Mermin ND. *Solid state physics*. Philadelphia: Saunders College, 1976.
7. Shoenberg, D. Magnetization of a two-dimensional electron gas. J Low Temp Phys 1984;56:417–40.
8. Miura N. *Physics of semiconductors in high magnetic fields*. New York: Oxford Science Publications, 2008.
9. Jain JK. *Composite fermions*. New York: Cambridge University Press, 2007.
10. Saminadayar L, Glattli DC, Jin Y, Etienne B. Observation of the e/3 fractionally charged Laughlin quasiparticle. Phys Rev Lett 1997;79:2526–29.
11. Seisyan RP, Zakharchenya BP. Interband optics of semiconductors as diamagnetic exciton spectroscopy. In: Landwehr G, Rashba EI, editors. *Landau level spectroscopy, modern problems in condensed matter sciences*, Volume 27.1. Amsterdam: North-Holland, 1991:344–43.
12. For a review with a discussion of some controversies, see Koch SW, Kira M, Khitrova G, Gibbs HM. Semiconductor excitons in new light. Nat Mater 2006; 5:523–31.
13. Rau ARP. *Astronomy-inspired atomic and molecular physics*. Dordrecht: Kluwer Academic, 2002.
14. Lai D. Matter in strong magnetic fields. Review of Modern Physics 2001;73:629–61.
15. Ashcroft NW, Mermin ND. *Solid State Physics*. Fort Worth: Harcourt College Publishers, 1976.
16. Nash KJ, Skolnick MS, Claxton PA, Roberts JS. Diamagnetism as a probe of exciton localization in quantum wells. Phys Rev B 1989;39:10943–54.
17. Elliott RJ, Loudon R. Theory of the absorption edge in semiconductors in a high magnetic field. J Phys Chem Solids1960;15:196–207.
18. Yafet Y, Keyes RW, Adams EN. Hydrogen atom in a strong magnetic field. J Phys Chem Solids 1956;1:137–42.
19. Zawadzki W. *Landau level spectroscopy*. Landwehr G, Rashba EI editor. Amsterdam: North Holland, 1991:1305.
20. Rosner W, Wunner G, Herold H, Ruder H. Hydrogen atoms in arbitrary magnetic fields. I. Energy levels and wavefunctions. J Physics B: Atomic and Molecular Phys 1984;17:447–62.
21. Xi J, He X, Li B. Energy levels of the hydrogen atom in arbitrary magnetic fields obtained by using B-spline basis sets. Phys Rev A 1992;46:5806–11.
22. Holle A, Main J, Wiebusch G, Rottke H, Welge KH. Quasi-Landau spectrum of the chaotic diamagnetic hydrogen atom. Phys Rev Lett 1998;61:161–4.
23. Thomas DG, Hopfield JJ. A magneto-stark effect and exciton motion in CdS. Phys Rev 1961;124:657–65.
24. Gor'kov LP, Dzyaloshinskii IE. Contribution to the theory of the Mott exciton in a strong magnetic field. Sov. Phys. JETP 1968;26:449–51.
25. Greene RL, Bajaj KK. Effect of magnetic field on the energy levels of a hydrogenic impurity center in GaAs/AlGaAs quantum-well structures. Phys Rev B 1985:31;913–8.
26. Haug H, Koch SW. *Quantum theory of the optical and electronic properties of semiconductors*, 4th Edition. Singapore: World Scientific, 2004.
27. Bayer M, Walck SN, Reinecke TL, Forchel A. Exciton binding energies and diamagnetic shifts in semiconductor quantum wires and quantum dots. Phys Rev 1998;57:6584–91.
28. Maan JC, Belle G, Fasolino A, Altarelli M, Ploog K, Magneto-optical determination of exciton binding energy in GaAs-$Ga_{1-x}Al_xAs$ quantum wells. Phys Rev 1984;30:2253–6.
29. MacDonald AH, Ritchie DS. Hydrogen energy levels in two dimensions at arbitrary magnetic fields. Phys Rev B 1986;33:8836–44.
30. Davies JH. *The physics of low-dimensional semiconductors: an introduction*. Cambridge: Cambridge University Press, 1998.
31. Vanhoucke T, Hayne M, Henini M, Moshchalkov VV. Magnetophotoluminescence of negatively charged excitons in narrow quantum wells. Phys Rev B 2001;63:125331.
32. Vanhoucke T, Hayne M, Henini M, Moshchalkov VV. Magnetic-field dependence of the spin states of the negatively charged exciton in GaAs quantum wells. Phys Rev B 2002;65:233305.
33. Wójs A, Quinn JJ, Hawrylak P, Charged excitons in a dilute two-dimensional electron gas in a high magnetic field. Phys Rev B 2000;62:4630–7.
34. Kuksuhkin IV, Timoveev VB. Magneto-optics of strongly correlated two dimensional electrons in single heterojunctions. Adv Phys 1996;45:147–242.
35. Potemski M. Magneto-optics of a two-dimensional electron gas. Physica B 1998;256–258;283–91.
36. Mlinar V, Schliwa A, Bimberg D, Peeters FM. Theoretical study of optical properties of inverted GaAs/$Al_xGa_{1-x}As$ quantum dots with smoothed interfaces in an external magnetic field. Phys Rev B 2007;75:205308.
37. Jacak L, Hawrylak P, Wójs A. *Quantum dots*. Berlin: Springer Verlag, 1998.
38. Schildermans N, Hayne M, Moshchlakov VV, Rastelli A, Schmidt O. Nonparabolic band effects in GaAs/$Al_xGa_{1-x}As$ quantum dots and ultrathin quantum wells. Phys Rev B 2005;72:15312.
39. Sidor Y, Partoens B, Peeters FM, Schildermans N, Hayne M, Moshchalkov, et al. High-field magnetoexcitons in unstrained GaAs/$Al_xGa_{1-x}As$ quantum dots. Phys Rev B 2006;73:155334.
40. Pryor C. Eight-band calculations of strained InAs/GaAs quantum dots compared with one-, four-, and six-band approximations. Phys Rev B 1998;57:7190–5.
41. Maes J. Magneto-photoluminescence of self-assembled InAs nanostructures [doctoral thesis]. Leuven, Belgium. Katholieke Universiteit Leuven, 2004.
42. Fock V. Bemerkung zur quantelung des harmonischen oszillators im magnetfeld. Z Phys 1928;47:446–8.
43. Darwin CG. The Diamagnetism of the Free Electron. Proc Cambridge Phil Soc 1931;27:86–90.
44. Hawrylak P. Excitonic artificial atoms: Engineering optical properties of quantum dots. Phys Rev B 1999;60:5597–608.
45. Babinski A, Potemski M, Raymond S, Lapointe J, Wasilewski ZR. Fock-Darwin spectrum of a single InAs/GaAs quantum dot. Phys stat sol (c) 2006;3:3748–51.
46. Miska P, Even J, Platz C, Salem B, Benyattau T, Bru-Chevalier C et al. Experimental and theoretical investigation of carrier confinement in InAs quantum dashes grown on InP (001). J Appl Phys 2004;95:1074–80.
47. Grundmann M, Stier O, Bimberg D. InAs/GaAs pyramidal quantum dots: Strain distribution, optical phonons and electronic structure. Phys Rev B 1995;52:11969–81.
48. Bester G, Zunger A. Cylindrically shaped zinc-blende semiconductor quantum dots do not have cylindrical symmetry: Atomistic symmetry, atomic relaxation, and piezoelectric effects. Phys Rev B 2005;71:045318.
49. Raymond S, Studenikin S, Sachrajda A, Wasilewski Z, Cheng SJ, Sheng W et al. Excitonic energy shell structure of self-assembled InGaAs/GaAs quantum dots. Phys Rev Lett 2004;92:187402.
50. Wang PD, Merz JL, Fafard S, Leon R, Leonard D, Mederios-Ribeiro G et al. Magnetopluminescence studies of $In_yAl_{1-y}As$ self-assembled quantum dots in $Al_xGa_{1-x}As$ matrices. Phys Rev B 1996;53:16458–61.
51. Rinaldi R, Giugno PV, Cingolani R, Lipsanen H, Sopanen M, Tulkki J et al. Zeeman Effect in Parabolic Quantum Dots. Phys Rev Lett 2006;77:342–5.
52. Walck SN, Reinecke TL. Exciton diamagnetic shift in semiconductor nanostructures. Phys Rev B 1998;57:9088–96.
53. Janssens KL, Peeters FM, Schweigert VA. Magnetic-field dependence of the exciton energy in a quantum disk. Phys Rev B 2001;63:205311.
54. It is interesting to note that this expression has the same functional form as one that is widely used to describe the temperature dependence of the energy gap in semiconductors. See Varshni YP. Temperature dependence of the energy gap in semiconductors. Physica 1967;34:149.

55. Hayne M, Provoost R, Zundel MK, Manz YM, Schmidt OG, Eberl K et al. Electron and hole confinement in stacked self-assembled InP quantum dots. Phys Rev 2000;62:10324–8.
56. Maes J, Hayne M, Moshchalkov VV, Patanè A, Henini M, Eaves L et al. Dependence of quantum-dot formation on substrate orientation studied by magnetophotoluminescence. Appl Phys Lett 2002;81:1480–2.
57. Maes J, Hayne M, Sidor Y, Peeters FM, González Y, González L et al. Electron wave-function spillover in self-assembled InAs/InP quantum wires [published erratum appears in Phys Rev B 2007;76:199902(E)]. Phys Rev B 2004;70:155311.
58. Hayne M, Maes J, Bersier S, Moshchalkov VV, Schliwa A, Müller-Kirsch L et al. Electron localization by self-assembled GaSb/GaAs quantum dots. Appl Phys Lett 2003;82:4355–7.
59. Bansal B, Hayne M, Geller G, Bimberg D, Moshchalkov VV. Excitonic Mott transition in type-II quantum dots. Phys Rev B 2008;77:241304 (R).
60. Cornet C, Hayne M, Levallois C, Caroff P, Joulaud L, Homeyer E et al. Phys Rev B 2006;74:245315.
61. Hayne M, Maes J, Manz YM, Schmidt OG, Moshchalkov VV. Magneto-photoluminescence study of type-II charge confinement in epitaxially grown $GaInP_2$. Physica E 2004;21:257–60.
62. Bansal B, Godefroo S, Hayne M, Medeiros-Riberio G, Moshchalkov VV. Extended excitons and compact heliumlike biexcitons in type-II quantum dots. Phys Rev B 2009;80:205317.
63. Godefroo S, Hayne M, Jivanescu M, Stesmans A, Zacharias M, Lebedev OI et al. Classification and control of the origin of photoluminescence from Si nanocrystals. Nat Nanotechnol 2008;3:174–8.
64. Nuytten T, Hayne M, Bansal B, Liu HY, Hopkinson M, Moshchalkov VV. Charge separation and temperature-induced carrier migration in $Ga_{1-x}InxN_yAs_{1-y}$ multiple quantum wells. Phys Rev B 2011;84:045302.
65. Note that by the argumentation presented, we expect this analysis to also be applicable to quantum wells. In particular, in Ref. 64 it was found that the electrons and holes in $Ga_{1-x}InxN_yAs_{1-y}$ quantum wells are spatially separated, so the two-dimensional hydrogen atom theory of Ref. 29 is not strictly valid anyway.
66. Hayne M, Maes J, Bersier S, Henini M, Müller-Kirch L, Heitz R et al. Pulsed magnetic fields as a probe of semiconductor nanostructures. Physica B 2004;346–7:421–7.
67. Vanacken J. The K.U. Leuven pulsed field facility solid state physics in high magnetic fields. Physica B 2001;294–294: 591–7.
68. Heiman D, Perry CH. *Magneto-optics of Semiconductors* in *High Magnetic Fields Science and Technology* Vol 2. Herlach F, Miura N editors. World Scientific: Singapore, 2003;47.
69. Pryor CE, Pistol M-E. Band-edge diagrams for strained III–V semiconductor quantum wells, wires, and dots. Phys Rev B 2005;72:205311.
70. Ribeiro E, Govorov AO, Carvalho Jr. W, Medeiros-Ribeiro G. Aharonov-Bohm signature for neutral polarized excitons in type-II quantum dot ensembles. Phys Rev Lett 2004;92:126402.
71. Maltez RL, Ribeiro E, Carvalho W, Ugarte D, Medeiros-Ribeiro G. Controlling alloy composition of InAsP self-assembled quantum dots embedded in GaAs. J Appl Phys 2003;94:3051–6.
72. Bimberg D, Grundmann M, Ledentsov NN. *Quantum dot heterostructures*. Chichester: Wiley, 1999.
73. Zundel MK, Specht P, Eberl K, Jin-Phillipp NY, Phillipp F. Structural and optical properties of vertically aligned InP quantum dots. Appl Phys Lett 1997;71:2972–4.
74. Tersoff J, Teichert C, Lagally MG. Self-Organization in growth of quantum dot superlattices. Phys Rev Lett 1996;76:1675–8.
75. Partoens B, Schweigert VA, Peeters FM. Classical double-layer atoms: artificial molecules. Phys Rev Lett 1997;79:3990–3.
76. Hu X, Das Sarma S. Hilbert-space structure of a solid-state quantum computer: two-electron states of a double-quantum-dot artificial molecule. Phys Rev A 2000;61:062301.
77. Luque A, Marti A. Increasing the efficiency of ideal solar cells by photon induced transitions at intermediate levels. Phys Rev Lett 1997;78:5014–7.
78. Le Ru EC, Howe P, Jones TS, Murray R. Strain-engineered InAs/GaAs quantum dots for long-wavelength emission. Phys Rev B 2003;67:165303.
79. Ledentsov NN, Shchukin VA, Grundmann M, Kirstaedter N, Böhrer J, Schmidt O et al. Direct formation of vertically coupled quantum dots in Stranski-Krastanow growth. Phys Rev 1996;54:8743–50.
80. Heinrichsdorff F, Mao M-H, Kirstaedter N, Krost A, Bimberg D, Kosogov AO et al. Appl Phys Lett 1997;71:22–4.
81. Maes J, Hayne M, Henini M, Pulizzi F, Patanè A, Eaves L et al. Magneto-photoluminescence of stacked self-assembled InAs/GaAs quantum dots. Physica B 2004;346–347:428–31.
82. Pryor C. Quantum Wires Formed from Coupled InAs/GaAs Strained Quantum Dots. Phys Rev Lett 1998;80:3579–81.
83. Ibáñez J, Patanè A, Henini M, Eaves L, Hernández S, Cusco R et al. Strain relaxation in stacked InAs/GaAs quantum dots studied by Raman scattering. Appl Phys Lett 2003;83:3069–71.
84. Frigeri P, Bosacchi A, Franchi S, Allegri P, Avanzini V. Vertically stacked quantum dots grown by ALMBE and MBE. J Crystal Growth 1999;201–201:1136–8.
85. Taddei S, Colocci M, Vinattieri A, Bogani F, Franchi S, Frigeri P et al. Vertical coupling and transition energies in multilayer InAs/GaAs quantum-dot structures. Phys Rev B 2000;62:10220–5.
86. Schmidt OG, Kienzle O, Hao Y, Eberl K, Ernst F. Modified Stranski–Krastanov growth in stacked layers of self-assembled islands. Appl Phys Lett 1999;74:1272–4.
87. Ball P. Let there be light. Nature 2001;409:974.
88. Canham LT. Silicon quantum wire array fabrication by electrochemical and chemical dissolution of wafers. Appl Phys Lett 1990;57:1046–8.
89. Lehmann V, Gösele U. Porous Si formation: A quantum wire effect. Appl Phys Lett 1991;58:856–8.
90. Heitmann J, Müller F, Zacharias M, Gosële U. Silicon nanocrystals: Size matters. Adv Mat 2005;17:795–803.
91. Gösele U. Shedding new light on silicon. Nat Nanotechnol 2008;3;134–5.
92. Delerue C, Allan G, Lanmoo, M. Theoretical aspects of the luminescence of porous silicon. Phys Rev B 1993;48:11024–36.
93. Delley B, Steigmeier EF. Quantum confinement in Si nanocrystals. Phys Rev B 1993;47:1397–400.
94. Ogüt S, Chelikowsky JR, Louie SG. Quantum confinement and optical gaps in Si nanocrystals. Phys Rev Lett 1997;79:1770–3.
95. Pudzer A, Williamson AJ, Grossman JC, Galli C. Surface chemistry of silicon nanoclusters. Phys Rev Lett 2002;88:097401.
96. Hadjisavvas G, Kelires PC. Structure and energetics of Si nanocrystals embedded in *a*-SiO_2. Phys Rev Lett 2004;93:226104.
97. Averboukh B, Huber R, Cheah KW, Shen YR, Qin GG, Ma ZC, Wong WH. Luminescence studies of a Si/SiO_2 superlattice. J Appl Phys 2002;92:3564–8.
98. Zacharias M, Heitmann J, Scholz R, Kahler U, Schmidt M, Bläsing J. Size-controlled highly luminescent silicon nanocrystals: A SiO/SiO_2 superlattice approach. Appl Phys Lett 2002;80:661–3.
99. Zimina A, Eisebitt S, Eberhardt W, Heitmann J, Zacharias M. Electronic structure and chemical environment of silicon nanoclusters embedded in a silicon dioxide matrix. Appl Phys Lett 2006;88:163103.
100. Abtew TA, Drabold DA. Atomistic simulation of light-induced changes in hydrogenated amorphous Si. J Phys Condens-Mat 2006;18:L1-L6.
101. Bansal B, Kadir A, Bhattacharya A, Moshchalkov VV. Photoluminescence from localized states in disordered indium nitride. Appl Phys Lett 2008;93:021113.
102. Hatami F, Ledentsov NN, Grundmann M, Böhrer J, Heinrichsdorff F, Beer M et al. Radiative recombination in type-II GaSb/GaAs quantum dots. Appl Phys Lett 1995;67:656–8.
103. Marent A, Geller M, Schliwa A, Feise D, Pötschke K, Bimberg D et al. 10^6 years extrapolated hole storage time in GaSb/AlAs quantum dots. Appl Phys Lett 2007;91:242109.
104. Tatebayashi J, Khoshakhlagh A, Huang SH, Balakrishnan G, Dawson LR, Huffaker D et al. Lasing characteristics of GaSb/GaAs self-assembled quantum dots embedded in an InGaAs quantum well. Appl Phys Lett 2007;90:261115.
105. Laghumavarapu RB, Moscho A, Khoshakhlagh A, El-Emawy M, Fester LF, Huffaker DL. GaSb/GaAs type II quantum dot solar cells for enhanced infrared spectral response. Appl Phys Lett 2007;90:173125.
106. Ahmad Kamarudin A, Hayne M, Young RJ, Zhuang QD, Ben T, Molina SI. Tuning the properties of exciton complexes in self-assembled GaSb/GaAs quantum rings. Phys Rev B 2011;83:115311.
107. Lin T-C, Li L-C, Lin S-D, Suen Y-W, Lee C-P. Anomalous optical magnetic shift of self-assembled GaSb/GaAs quantum dots. J Appl Phys 2011;110:013522.
108. Ledentsov NN, Böhrer J, Beer M, Heinrichsdorff F, Grundmann M, Bimberg D et al. Radiative states in type-II GaSb/GaAs quantum wells. Phys Rev B 1995;52:14058–14066.
109. Müller-Kirsch L, Heitz R, Schliwa A, Bimberg D, Kirmse H, Neumann W. Many-particle effects in type II quantum dots. Appl Phys Lett 2001;78:1418–20.

110. Hayne M, Razinkova O, Bersier S, Heitz R, Müller-Kirsch L, Geller M et al. Optically induced charging effects in self-assembled GaSb/GaAs quantum dots. Phys Rev B 2004;70:081302[R].
111. Kappei L, Szczytko J, Morier-Genoud F, Deveaud. Direct observation of the Mott transition in an optically excited semiconductor quantum well. Phys Rev Lett 2005;94:147403.
112. Alen B, Fuster D, Munoz-Matutano G, Martinez-Pastor J, Gonzalez Y, Canet-Ferrer J et al. Exciton gas compression and metallic condensation in a single semiconductor quantum wire. Phys Rev Lett 2008;101:067405.
113. Nuytten T, Hayne M, Henini M, Moshchalkov VV. Temperature dependence of the photoluminescence of self-assembled InAs/GaAs quantum dots in pulsed magnetic fields. Phys Rev B 2008;77:115348.